Supporting Information

Photophysical Properties of Co(III) Photosensitizers with Phenothiazine-based Ligands

*Jessica Toigo[a], Ka-Ming Tong[a], Saied Kamal[a], Charles J. Walsby[b], Brian O. Patrick[a], Michael O. Wolf[a]**

[a] Department of Chemistry, University of British Columbia, Vancouver, British Columbia V6T 1Z1, Canada

[b] Department of Chemistry, Simon Fraser University, Burnaby, British Columbia, V5A 1S6, Canada

Table of Contents	**Page**

General experiments were conducted under inert nitrogen atmosphere using standard Schlenk techniques unless otherwise stated. De-gassed, purified, and dry tetrahydrofuran (THF), dichloromethane and DMSO were obtained from an Innovative Technology Inc. solvent purification system (SPS) and stored in an oven-dried Schlenk bomb. All reagents were obtained from Sigma-Aldrich, Alfa Aesar, Ambeed Inc. or Thermo Scientific and used without additional purification. HPLC grade solvents were used for spectroscopic studies.

High-resolution electrospray ionization (HR-ESI) mass spectrometry data were obtained on a Waters/Micromass LCT TOF-MS spectrometer.

Fourier transform infrared (FT-IR) spectroscopy was performed using an attenuated total reflection (ATR) crystal on a PerkinElmer Frontier FT-IR spectrometer.

Nuclear magnetic resonance (NMR) experiments were recorded on Bruker AVIII HD 400 MHz, Bruker Avance 400 MHz, and Bruker Neo 600 MHz spectrometers; ^{1}H and $^{13}C\{^{1}H\}$ NMR chemical shifts (δ) are given in parts per million (ppm) relative to TMS, using the residual solvent signal for calibration. $^{31}P\{^{1}H\}$ NMR was calibrated using 85% H_3PO_4 as external standard. $^{19}F\{^{1}H\}$ was calibrated using trifluoroacetic acid (TFA) as external standard. NMR solvent from Cambridge Isotope Laboratories was used as received.

X-band electron paramagnetic resonance (EPR) spectra were collected on a Bruker EMXplus spectrometer with a PremiumX microwave bridge and HS resonator at room temperature. EPR spectra were simulated using EasySpin on MATLAB.[1]

X-ray Crystallography data was collected using a Bruker APEX DUO diffractometer with graphite monochromated Mo Kα radiation (λ = 0.71073 Å) at 100 K. Raw frame data were processed using APEX4. The program SAINT[2] was used to reduce the data and the program SADABS[3] was used to make corrections to the empirical absorptions. Space group assignments were made using XPREP. The structure was solved in the Olex2[4] suite of programs using Intrinsic Phasing and refined using full-matrix least-squares/difference Fourier techniques on F2 using SHELXL.[5] All non-hydrogen atoms

were refined anisotropically. Diagrams and publications materials were generated using ORTEP-3, Mercury and PLATON.

UV-vis absorption spectra were obtained on a Varian-Cary 5000 UV-vis-near-IR spectrophotometer.

Photoluminescence spectra at room temperature were collected using an Edinburgh Instrument FLS1000 spectrofluorometer. Solution samples were maintained under a blanket of Ar for the duration of the measurements in 1 cm^2 quartz cells (Starna Cells).

Emission lifetime data at room temperature were obtained using an Edinburgh Instruments 365 nm EPLED excitation source, time-correlated single-photon counting (TCSPC), and a 400 nm long-pass filter between the sample and detector.

Photoluminescence quantum yields of the solution samples were determined using an Edinburgh Instruments barium sulfate-coated integrating sphere fitted in an FS5 spectrofluorometer with optical densities less than 0.1.

Cyclic voltammograms were recorded using a Pine AFCBP1 potentiostat with a 3-electrode configuration using a Pt working electrode, Ag wire reference electrode and Pt mesh counter electrode. 0.1 mol L^{-1} (^{n}Bu_4N)PF_6 in acetonitrile was degassed with Ar and used as the electrolyte. 0.1 mmol L^{-1} solutions of each sample were prepared, and a scan rate of 100 mV s^{-1} was applied in all cases. Potentials were referenced to $Fc^{+/0}$ with the addition of ferrocene at the end of each experiment.

Spectroelectrochemical measurements were carried out on an Autolab pgstat12 electrochemical analyzer using a room temperature optically transparent thin-layer electrochemical (OTTLE) cell. 3-electrode system of Au minigrid (32 wires/cm) working electrode, Pt wire auxiliary electrode and an Ag wire pseudoreference electrode was used.[6] Experiments were conducted from open circuit potential to the set potential at a scan rate of 10 mV s^{-1}. Open circuit potential was applied for 60 seconds before every scan. Spectral changes during oxidations/reductions were recorded on a Varian-Cary 5000 UV-vis-near-IR spectrophotometer.

Femtosecond transient absorption (fsTA) experiments were performed using a Newport pump-probe femtosecond transient absorption spectroscopy system. This system employs an amplified Ti:sapphire femtosecond laser (Legend, Coherent) with an output at 800 nm, with a pulse duration of 120 fs, pulse energy of 2 mJ, and repetition rate of 1 kHz. A portion of the laser output (1 mJ) was frequency-doubled to 400 nm using a BBO crystal via second harmonic generation (SHG) and used as the excitation (pump) beam. This introduces a discontinuity in the data, observed as a gap in the difference absorbance spectra. Probe pulses are generated by focusing a fraction of the 800 nm laser beam onto a 2 mm thick CaF_2 disk, producing a white light continuum spanning from 350 nm to 700 nm. Both pump and probe beams are directed onto the sample with their relative polarization adjusted to the magic angle, while a delay stage (Newport, DL325) controls the timing of the probe pulses. The pump pulses were modulated at 500 Hz by an optical chopper, and the probe spectra were recorded with a spectrograph (Oriel, MS260) and a CCD camera (S10453-1024Q, Hamamatsu). Global analysis of the fsTA data is performed using the open-source software Glotaran. Solution of complexes was dissolved in acetonitrile inside the glovebox, and the sample solution was filled into a fused-silica cuvette with a thickness of 2 mm. All measurements were recorded at room temperature unless stated otherwise.

Quantum chemical calculations were carried out using density functional theory (DFT) in with the Orca 6.0.1 software package.[7] The B3LYP functional[8,9] with basis set ZORA-def2-TZVP for Co(III) atom,[10] and the ZORA-def2-SVP[11] for the other atoms was employed to optimize the geometry of the ground states (S_0) and lowest-energy triplet states (T_1). Tight convergence criteria were used for optimizations calculations (keywords *tightopt* and *tightscf*). Dispersion effects were included using Grimme's D3 correction with Becke-Johnson (BJ) damping. The calculation of four-center integrals was accelerated using the RIJCOSX algorithm, which required an auxiliary basis set (SARC/J) for the Coulomb interaction and a numerical integration grid (DefGrid-2) for the exchange interaction.[12,13] Solvent correction was included using the linear response conductor-like polarizable continuum model (LR-CPCM) method, with acetonitrile as the solvent.[14] Analytical harmonic vibrational frequency calculations were performed to confirm that the ground state represents the lowest energy point on

the potential energy surface. Simulations of the absorption spectra were obtained using time-dependent density functional theory (TD-DFT) without the Tamm-Dancoff Approximation (TDA *false*).[15] The first 50 excitations were obtained using the same calculation protocol. Quasi-degenerate perturbation theory was utilized to conduct the SOC calculations in addition to the TD-DFT results.[16] The geometric representations of the compounds were plotted using the Chemcraft 1.8 program.[17]

Synthetic route

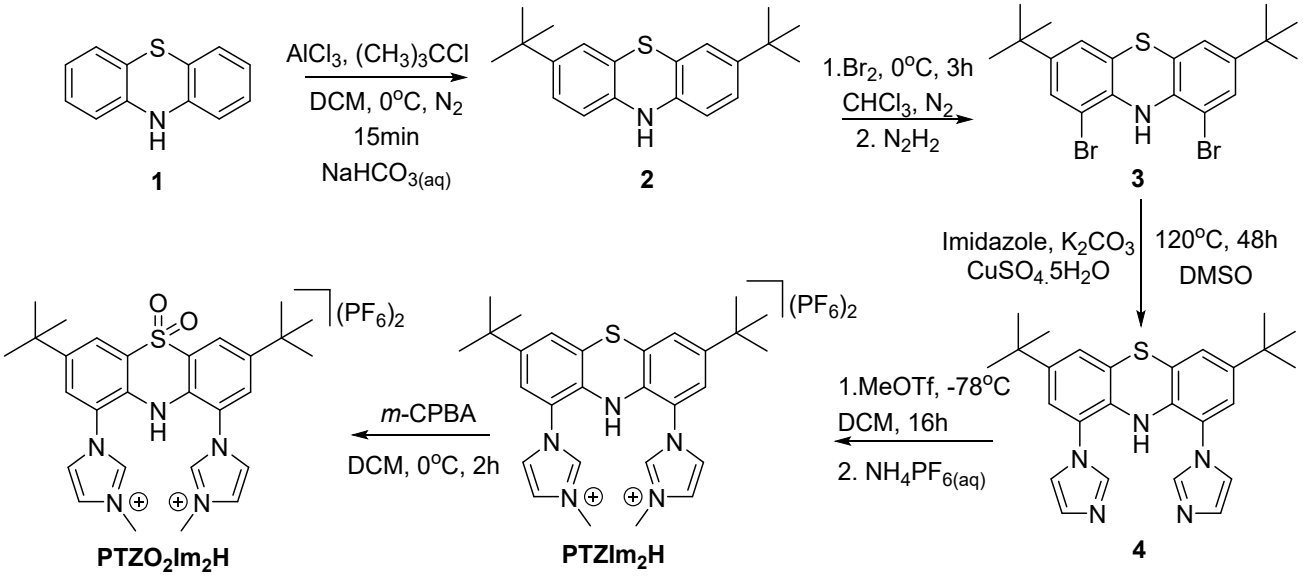

Scheme S1. Synthesis of the ligand precursors.

Synthesis of compound 2. Compound **2** was synthesized following a modified literature procedure.[18]

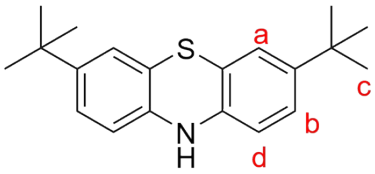

In a 250 mL Schlenk flask, phenothiazine **1** (10.0 g, 50.2 mmol, 1 eq) and anhydrous $AlCl_3$ (14.0 g, 105.4 mmol, 2.1 eq) were suspended in 50 mL of dry dichloromethane at 0°C. 2-Chloro-2-methylpropane (27.5 mL, 255.6 mmol, 5 eq) was added dropwise to the mixture. After the addition, the reaction was left stirring for 15 min at 0°C. The resulting red mixture was poured into a saturated aqueous solution of $NaHCO_3$. The phases were separated, and the aqueous phase was extracted with dichloromethane (3 × 50 mL). The combined organic phases were washed with a saturated sodium dithionite solution, and the solution changed in color from red to yellow. The organic phase was dried over magnesium sulfate, filtered, and the solvent was removed under reduced pressure. The crude product was washed with *n*-hexane and dried in vacuo. Compound **2** was obtained as a colorless solid (15.2 g, 48.8 mmol, 97 %) that slowly turns pink upon exposure to air. ^{1}H NMR (400 MHz, CD_2Cl_2) δ 7.02 (m, 4H, H_b, H_d), 6.53 (m, 2H, H_a), 1.25 (s, 18H, H_c). The spectral analytical data are consistent with those reported in the literature.[18]

Synthesis of compound 3. Compound **3** was synthesized following a modified literature procedure.[18]

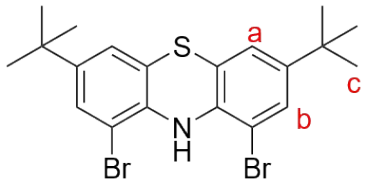

In a 100 mL Schlenk flask, compound **2** (1.1 g, 3.6 mmol, 1.0 eq) was dissolved in anhydrous and degassed chloroform (15 mL). Bromine (0.7 mL, 13.1 mmol, 3.6 eq) was added dropwise to the red solution at 0°C within 10 minutes. The mixture was stirred for 2.5 hours at room temperature. The resulting dark mixture was diluted with 10 mL of chloroform. The reaction was quenched by the addition of hydrazine monohydride (1.4 mL, 28.0 mmol) followed by the addition of 25 mL of saturated Na_2CO_3 solution. The phases were separated, and the aqueous phase was extracted with dichloromethane (2 × 20 mL). The combined organic phases were washed with brine (2 × 30 mL) and dried over magnesium sulfate. The solution was filtered, and the solvent was evaporated under reduced pressure. The product was purified through a flash column using dichloromethane as the solvent. Compound **3** was obtained as an off-white solid. (1.3 g, 2.8 mmol, 78%). ^{1}H NMR (400 MHz, CD_2Cl_2) δ 7.28 (d, J = 2.1 Hz, 2H, H_b), 7.07 (s, 1H, NH), 6.98 (d, J = 2.0 Hz, 2H, H_a), 1.24 (s, 18H, H_c). The spectral analytical data are consistent with those reported in the literature.[18]

Synthesis of compound 4. Compound **4** was synthesized following a modified literature procedure.[19]Compound **3** (1.5 g, 3.3 mmol, 1.0 eq), potassium carbonate (2.7 g, 19.2 mmol, 6.0 eq), imidazole (1.3 g, 19.2 mmol, 6.0 eq), and $CuSO_4 \cdot 5H_2O$ (159.0 mg, 0.7 mmol, 0.2 eq) were added to a 15 mL sealed tube. 5 mL of dry dimethyl sulfoxide was added. The tube was sealed and heated at 120°C for 48 hours under nitrogen. The reaction was quenched by the addition of 10 mL of saturated NH_4Cl solution followed by 100 mL of water. The mixture was extracted with dichloromethane (3 × 50 mL). The combined organic phase was washed with water (3 × 50 mL) and dried over magnesium sulfate. The solution was filtered, and the solvent was evaporated under reduced pressure. Compound **4** was obtained as an off-white solid after crystallization in ethyl acetate. (0.874 g, 1.97 mmol, 60%). ^{1}H NMR (400 MHz, $CDCl_3$) δ 7.44 (s, 2H, H_d), 7.15 (s, 2H, H_f), 7.12 (d, J = 2.1 Hz, 2H, H_b), 6.92 (d, J = 2.1 Hz, 2H, H_a), 6.74 (s, 2H, H_e), 5.65 (s, 1H, NH), 1.26 (s, 18H, H_c). ^{13}C NMR (151 MHz, $CDCl_3$) δ 146.9,

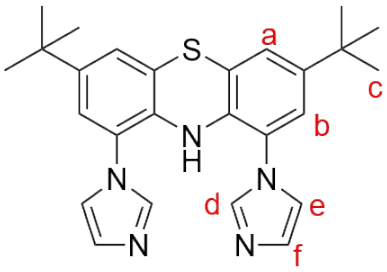

137.5, 134.1, 131.5, 124.7, 123.5, 122.6, 119.8, 118.9, 34.5, 31.2. HRMS (ESI, positive ions): m/z 444.2222 (calcd for $[C_{26}H_{30}N_5S]^+$ 444.2216).

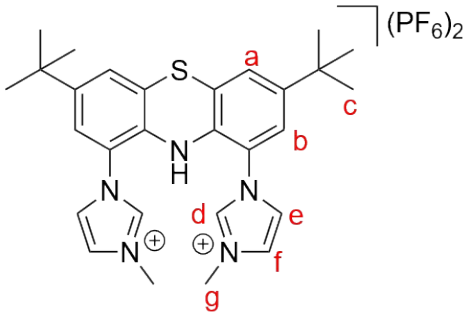

Synthesis of ligand $PTZIm_2H$. In a 50 mL Schlenk flask, compound **4** (0.3 g, 0.8 mmol, 1.0 eq) was dissolved in 15 mL of dry dichloromethane and cooled to −78°C. Methyl trifluoromethanesulfonate (180.6 µL, 1.6 mmol, 2.0 eq) was added dropwise to the solution. The reaction was stirred for 16 h, allowing it to reach room temperature. The reaction was quenched by the addition of 20 mL of *n*-pentane at 0°C. The product was then filtered and washed with cold *n*-pentane. The crude product was dissolved in a small amount of acetone and precipitated into a saturated aqueous solution of KPF_6. The final product was filtered and washed with diethyl ether. **$PTZIm_2H$** was obtained as a light-yellow solid that was recrystallized in methanol and slowly turns green upon exposure to air. (0.46 g, 0.63 mmol, 79%). ^{1}H NMR (600 MHz, CD_3CN) δ 8.53 (m, 2H, H_d), 7.46 (t, J = 1.8 Hz, 2H, H_f), 7.40 (t, J = 1.8 Hz, 2H, H_e), 7.29 (d, J = 2.2 Hz, 2H. H_b), 7.10 (d, J = 2.1 Hz, 2H, H_a), 6.11 (s, 1H, NH), 3.90 (s, 6H, H_g), 1.26 (s, 18H, H_c).^{13}C NMR (151 MHz, CD_3CN) δ 148.3, 139.0, 134.0, 127.1, 125.4, 124.8, 124.6, 122.8, 122.2, 37.1, 35.2, 31.1. HRMS (ESI, positive ions): m/z 236.6299 (calcd for $[PTZIm_2H]^{2+}$ 226.6301).

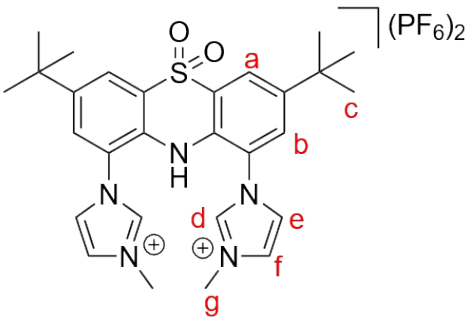

Synthesis of ligand $PTZO_2Im_2H$. In a 50 mL rbf, under air, **$PTZIm_2H$** (0.3 g, 0.5 mmol, 1.0 eq) was dissolved in 10 mL of DCM and cooling to 0°C. *m*-CPBA 77% (0.2 g, 1.0 mmol, 2.2 eq) was dissolved in 5 mL and added dropwise to the solution, resulting in a change in the color of the solution to bright yellow. The reaction was stirred for 2 hours while allowing it to reach room temperature. Saturated aqueous sodium carbonate solution was added, and the phases were separated. The aqueous phase was extracted with DCM (3 × 50 mL). The organic phase was dried over magnesium sulfate, filtered, and the solvent was removed under reduced pressure. **$PTZO_2Im_2H$** was obtained as a bright yellow solid that was recrystallized in ethanol (0.273 g, 0.34

mmol, 75 %). ^{1}H NMR (600 MHz, CD_3CN) δ 8.69 (s, 2H, H_d), 8.23 (d, J = 2.2 Hz, 2H, H_a), 8.08 (s, 1H, NH), 7.82 (d, J = 2.2 Hz, 2H, H_b), 7.53 (t, J = 1.9 Hz, 2H, $H_{e/f}$), 7.51 (t, J = 1.9 Hz, 2H, $H_{e/f}$), 3.94 (s, 6H, H_g), 1.39 (s, 18H, H_c). ^{13}C NMR (151 MHz, CD_3CN) δ 148.4, 139.5, 132.4, 131.8, 125.8, 125.6, 125.0, 123.71, 122.7, 37.2, 35.9, 31.0. HRMS (ESI, positive ions): m/z 252.6254 (calcd for $[PTZO_2Im_2H]^{2+}$ 226.6250); 504.2427 (calcd for $[PTZO_2Im_2H]^{+}$ 504.2428).

Synthesis of CoS. In a 50 mL Schlenk flask, **$PTZIm_2H$** (200.0 mg, 0.3 mmol, 2 eq) was dissolved in 10 mL of THF, and the suspension was cooled to −78°C. LiHMDS (165.0 mg, 1.0 mmol, 6.6 eq) in 5 mL of THF was added dropwise and stirred for 2 hours to ensure full deprotonation of the ligand. A solution of 33 mg of $CoBr_2$ (0.15 mmol, 1.0 eq) in 5 mL of dry THF was added dropwise at −78°C over a period of 10 minutes. The reaction was warmed to room temperature and left overnight, affording a dark green solution. The reaction was opened to the air and stirred for 30 minutes to promote the oxidation of Co(II) to Co(III). The solvent was removed under reduced pressure. A minimum amount of acetone was added, and the solution was filtered through Celite. The solution was concentrated and precipitated in a saturated aqueous solution of KPF_6. The solid was filtered and washed with diethyl ether. The compound was purified through silica column chromatography using dichloromethane/methanol (95:5) as the eluent. The green solid was reduced using sodium dithionite and stored in the glovebox to yield a reduced brown solid (114 mg, 0.1 mmol, 34%). ^{1}H NMR (600 MHz, Acetone) δ 7.77 (s, 2H), 7.69 (s, 2H), 7.50 (s, 2H), 7.23 (s, 2H), 7.03 (s, 2H), 6.73 (s, 2H), 6.61 (s, 2H), 6.46 (s, 2H), 4.02 (s, 6H), 3.35 (s, 6H), 1.36 (s, 18H), 1.23 (s, 18H). ^{13}C{^{1}H} NMR (151 MHz, Acetone) δ 174.5, 161.8, 143.7, 143.2, 141.8, 140.4, 129.9, 129.5, 129.1, 128.0, 127.0, 123.2, 121.7, 121.1, 120.0, 118.1, 114.5, 40.0, 39.7, 34.6, 34.5, 31.8, 31.5. ^{31}P{^{1}H} NMR (162 MHz, Acetone) δ −142.7 (sept, J = 707.9 Hz). ^{19}F{^{1}H} NMR (377 MHz, CD_3CN) δ −70.3 (d, J = 708.8 Hz). HRMS (ESI, positive ions): m/z 999.4085 (calcd for $[Co(PTZIm_2)_2]^{+}$ 999.4089).

Synthesis of $CoSO_2$. In a 50 mL Schlenk flask, **$PTZO_2Im_2H$** (160.0 mg, 0.2 mmol, 2.0 eq) was dissolved in 10 mL of THF, and the suspension was cooled down to −78°C. LiHMDS (111.0 mg, 0.66 mmol, 6.6 eq) in 5 mL of THF was added dropwise and stirred for 2 hours to ensure full deprotonation of the ligand. A solution of 33 mg of $CoBr_2$ (22.0 mg, 0.1 mmol, 1.0 eq) in 5 mL of dry

THF was added dropwise at −78°C over a period of 10 minutes. The reaction was warmed to room temperature overnight, affording a dark brown solution. The reaction was opened to the air and stirred for 30 minutes to promote the oxidation of Co(II) to Co(III). The solvent was removed under reduced pressure. A minimum amount of acetone was added, and the solution was filtered through Celite. The solution was concentrated and precipitated in a saturated aqueous solution of KPF_6. The solid was filtered and washed with methanol and diethyl ether, yielding an orange solid (106.0 mg, 0.1 mmol, 44%). Single crystals were obtained from vapour diffusion of *n*-pentane into a dichloromethane solution of **$CoSO_2$**. ^{1}H NMR (600 MHz, CD_3CN) δ 7.67 (d, J = 2.1 Hz, 2H), 7.63 (d, J = 2.2 Hz, 2H), 7.59 (d, J = 2.2 Hz, 2H), 7.44 (d, J = 2.1 Hz, 2H), 7.37 (d, J = 2.2 Hz, 2H), 7.36 (d, J = 2.1 Hz, 2H), 7.25 (d, J = 2.1 Hz, 2H), 7.00 (d, J = 2.1 Hz, 2H), 3.58 (s, 6H), 3.42 (s, 6H), 1.38 (m, 36H). ^{13}C{^{1}H} NMR (151 MHz, CD_3CN) δ 169.3, 160.3, 143.0, 142.7, 140.8, 137.72 131.8, 129.8, 129.2, 127.2, 126.4, 126.4, 125.7, 124.8, 123.1, 120.7, 120.0, 117.8, 39.4, 35.3, 31.4, 31.2. ^{31}P{^{1}H} NMR (162 MHz, CD_3CN) δ −143.1 (sept, J = 707.9 Hz). ^{19}F{^{1}H} NMR (377 MHz, CD_3CN) δ −73.5 (d, J = 708.8 Hz). HRMS (ESI, positive ions): m/z 1063.3883 (calcd for $[Co(PTZO_2Im_2)_2]^+$ 1063.3885).

Synthesis of FeS. In a 50 mL Schlenk flask, **$PTZIm_2H$** (153.0 mg, 0.2 mmol, 2.0 eq) was added 10 mL of THF, and the suspension was cooled down to −78°C. LiHMDS (111.0 mg, 0.66 mmol, 6.6 eq) in 5 mL of THF was added dropwise and stirred for 2 hours to ensure fully deprotonation of the ligand. A solution of 33 mg of $FeBr_2$ (29 mg, 0.1 mmol, 1.0 eq) in 5 mL of dry THF was added dropwise at −78°C. The reaction was left to warm to room temperature overnight, affording a dark green solution. The reaction was opened to the air and stirred for 30 minutes to promote the oxidation of Fe(II) to Fe(III). The solvent was removed under reduced pressure. The crude product was dissolved in a small amount of acetone and precipitated in a saturated aqueous solution of KPF_6. The solid was filtered and washed with ethanol, yielding a dark green solid (33.0 mg, 0.03 mmol, 29%). HRMS (ESI, positive ions): m/z 994.4051 (calcd for $[Fe(PTZIm_2)_2]^+$ 994.4153).

Synthesis of $FeSO_2$. In a 50 mL Schlenk flask, **$PTZO_2Im_2H$** (160.0 mg, 0.2 mmol, 2.0 eq) was dissolved in 10 mL of THF, and the suspension was cooled down to −78°C. LiHMDS (111.0 mg, 0.66 mmol, 6.6 eq) in 5 mL of THF was added dropwise and stirred for 2 hours to ensure fully deprotonation

of the ligand. A solution of 33 mg of $FeBr_2$ (30.0 mg, 0.1 mmol, 1.0 eq) in 5 mL of dry THF was added dropwise at −78°C. The reaction was left to warm to room temperature overnight, affording a dark green solution. The reaction was opened to the air and stirred for 30 minutes to promote the oxidation of Fe(II) to Fe(III). The solvent was removed under reduced pressure. The crude product was dissolved in a small amount of acetone and precipitated in a saturated aqueous solution of KPF_6. The solid was filtered and washed with methanol, yielding a bright green solid (42.0 mg, 0.04 mmol, 35%). Single crystals were obtained from vapour diffusion of *n*-pentane into a dichloromethane solution of **$FeSO_2$**. HRMS (ESI, positive ions): m/z 1058.3953 (calcd for $[Fe(PTZO_2Im_2)_2]^+$ 1063.3950).

FT-IR spectroscopy data

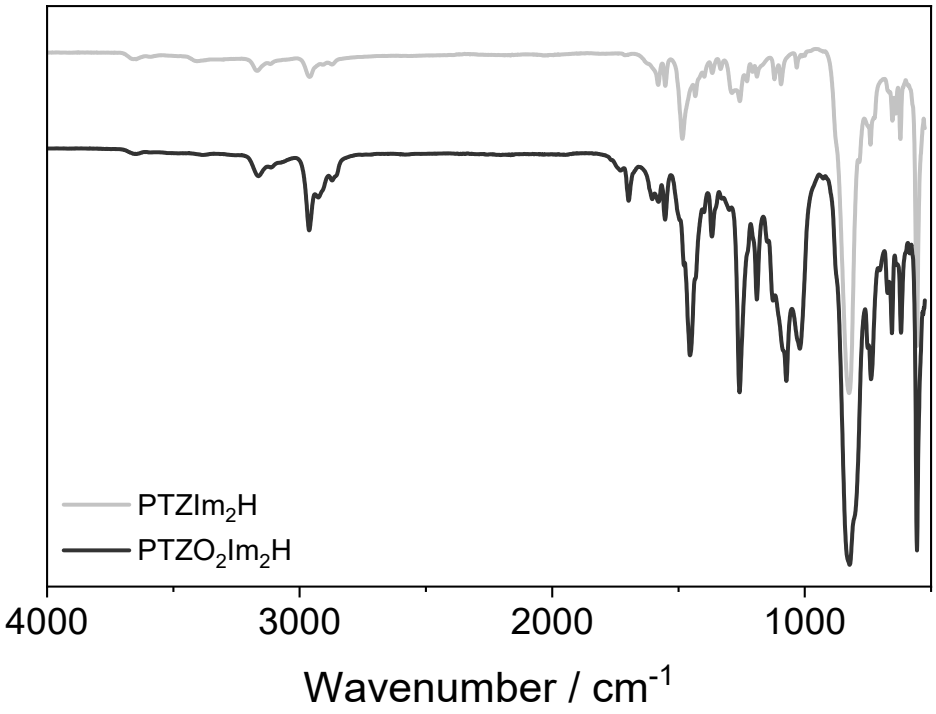

Figure S1. FT-IR spectra of ligands **$PTZIm_2H$** and **$PTZO_2Im_2H$.**

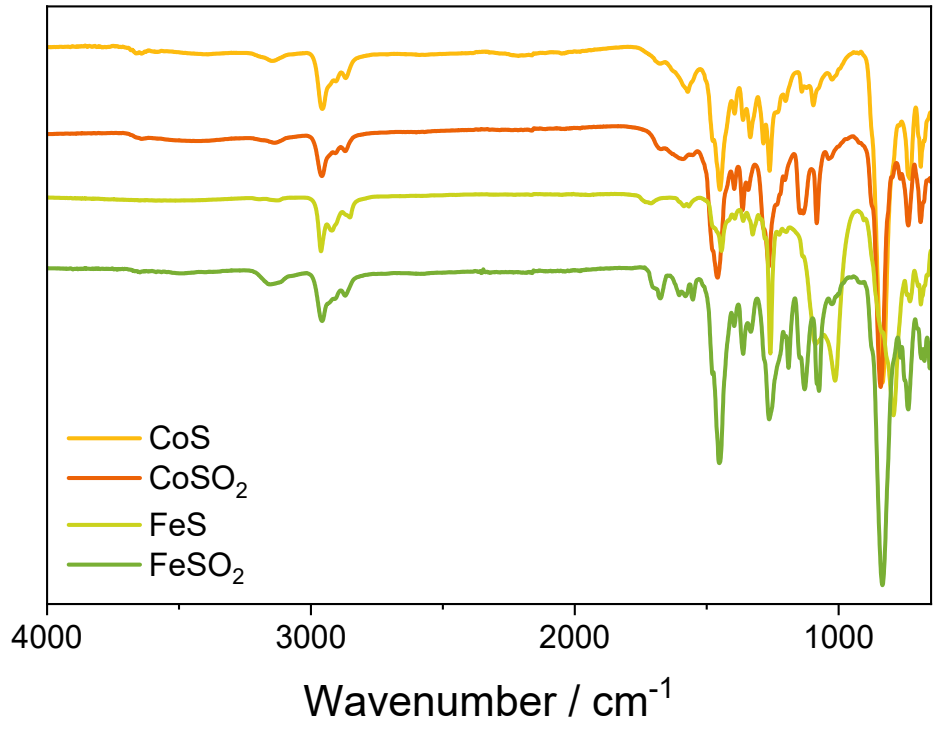

Figure S2. FT-IR spectra of complexes **CoS**, **$CoSO_2$**, **FeS** and **$FeSO_2$.**

Mass spectrometry data

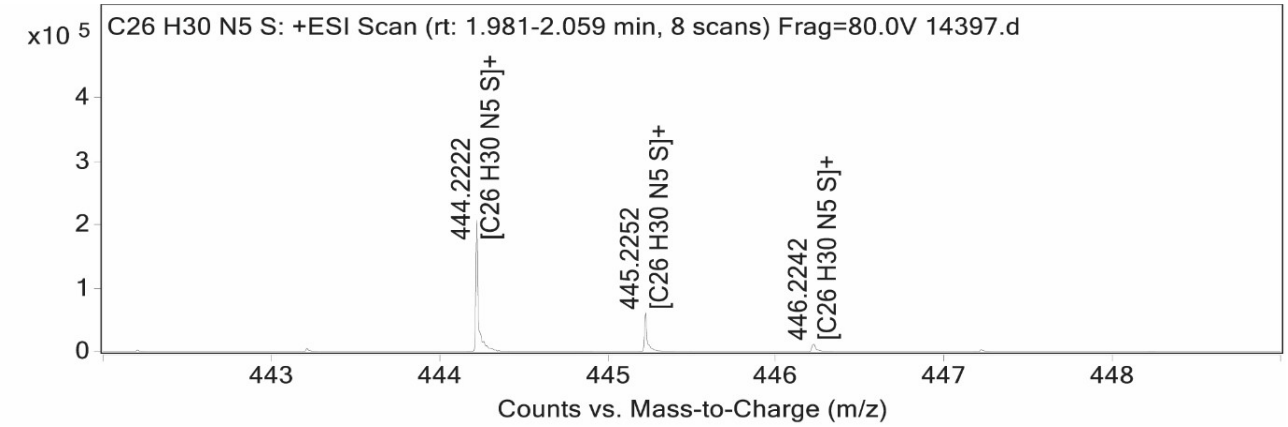

Figure S3. HR-ESI (positive ions) mass spectrum of **4**.

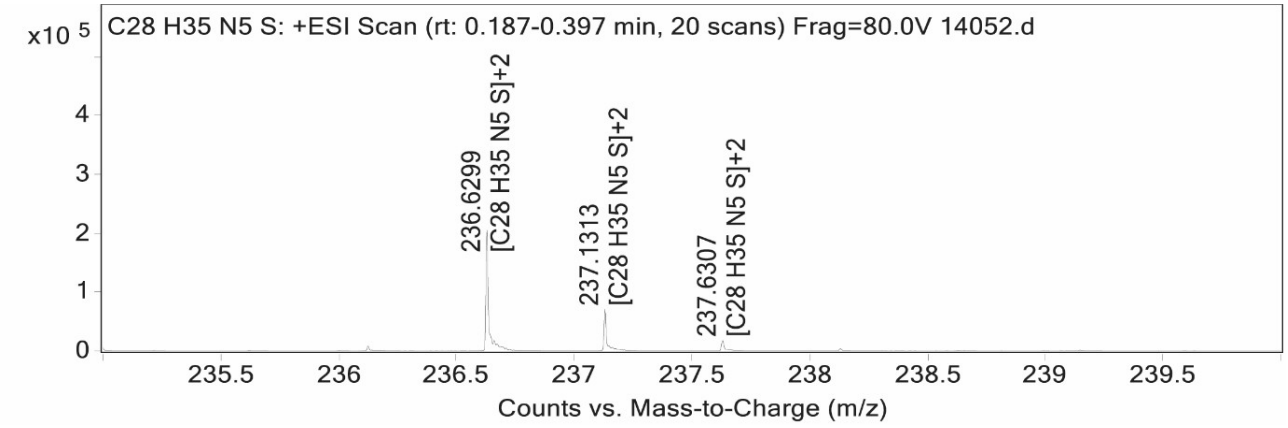

Figure S4. HR-ESI (positive ions) mass spectrum of **$PTZIm_2H$**.

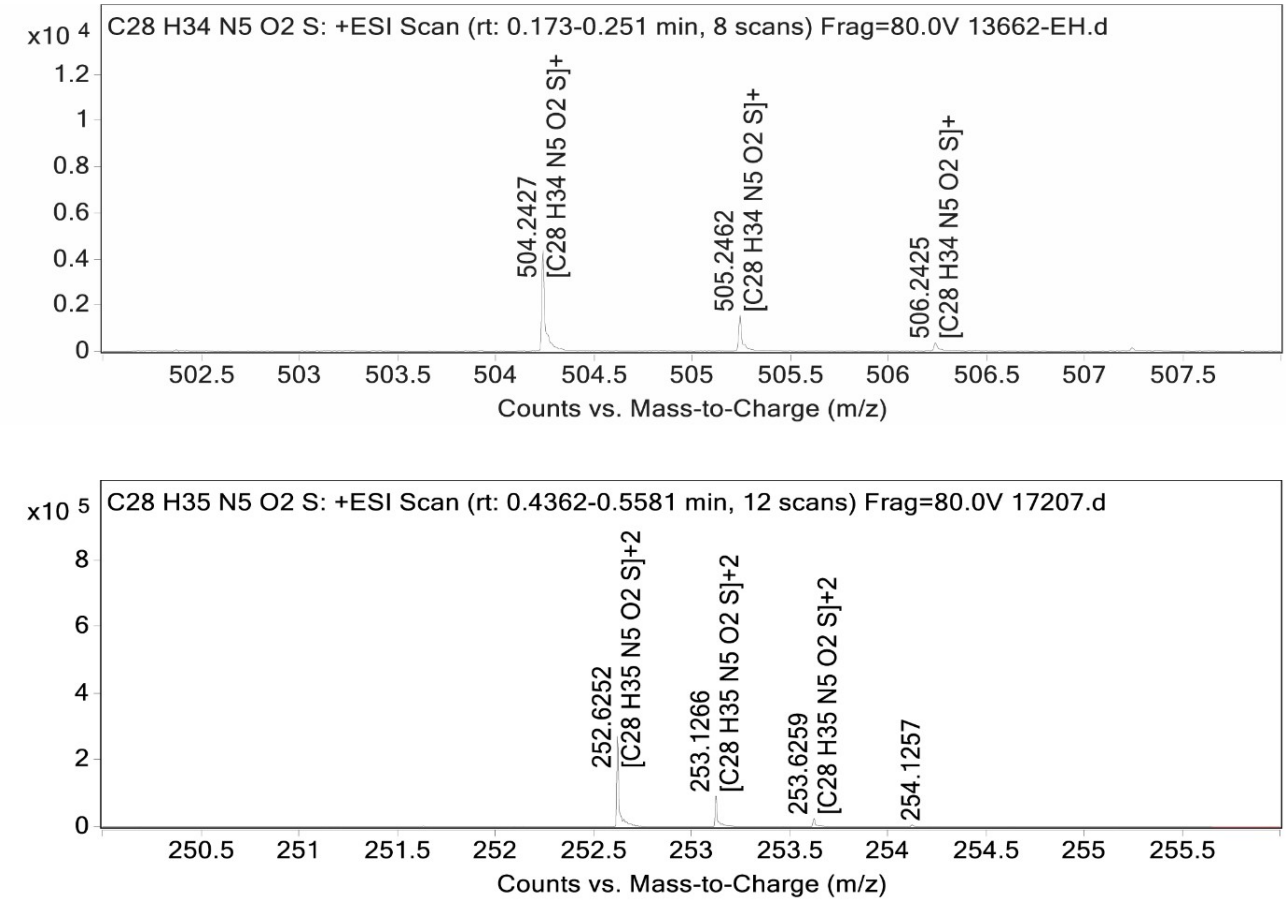

Figure S5. HR-ESI (positive ions) mass spectrum of **$PTZO_2Im_2H$**.

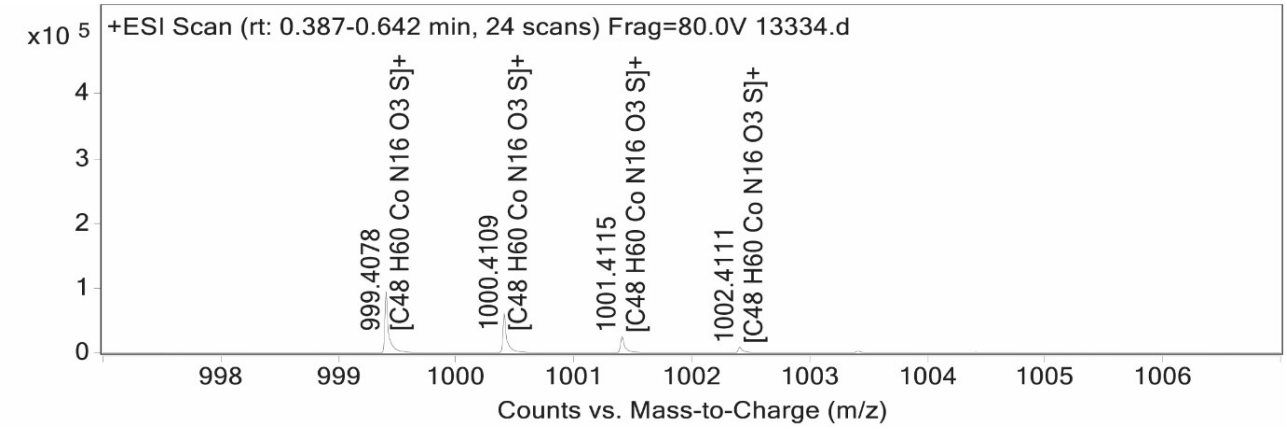

Figure S6. HR-ESI (positive ions) mass spectrum of **CoS**.

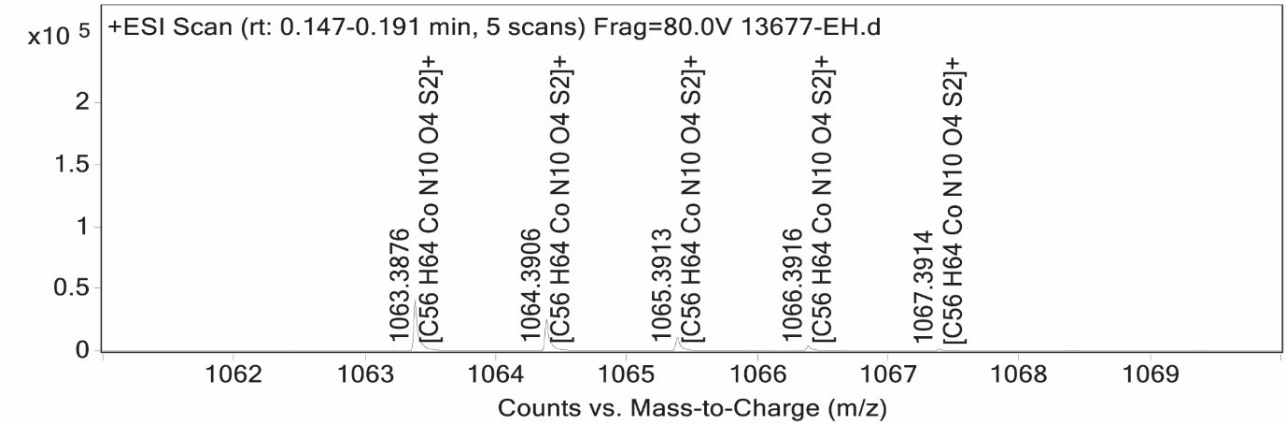

Figure S7. HR-ESI (positive ions) mass spectrum of **$CoSO_2$**.

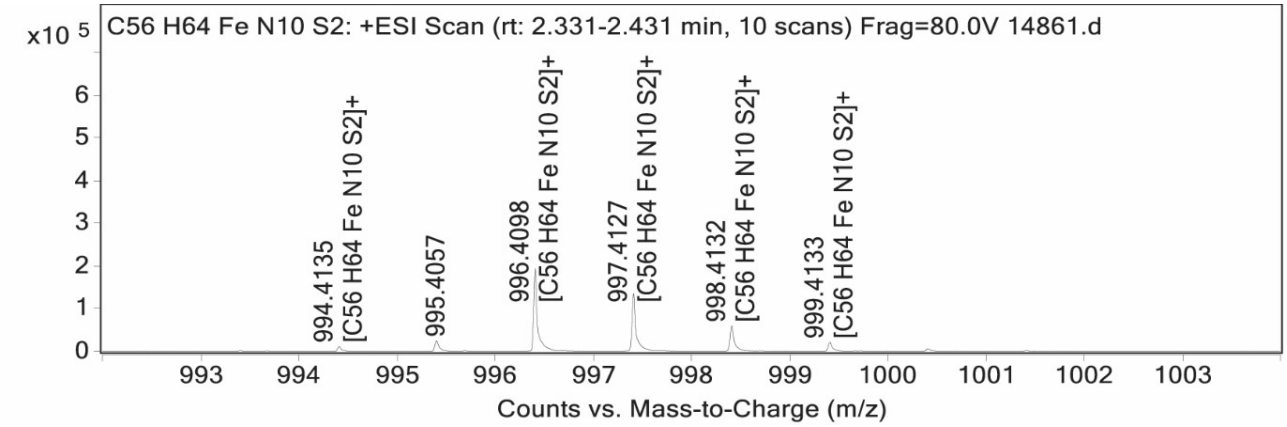

Figure S8. HR-ESI (positive ions) mass spectrum of **FeS**.

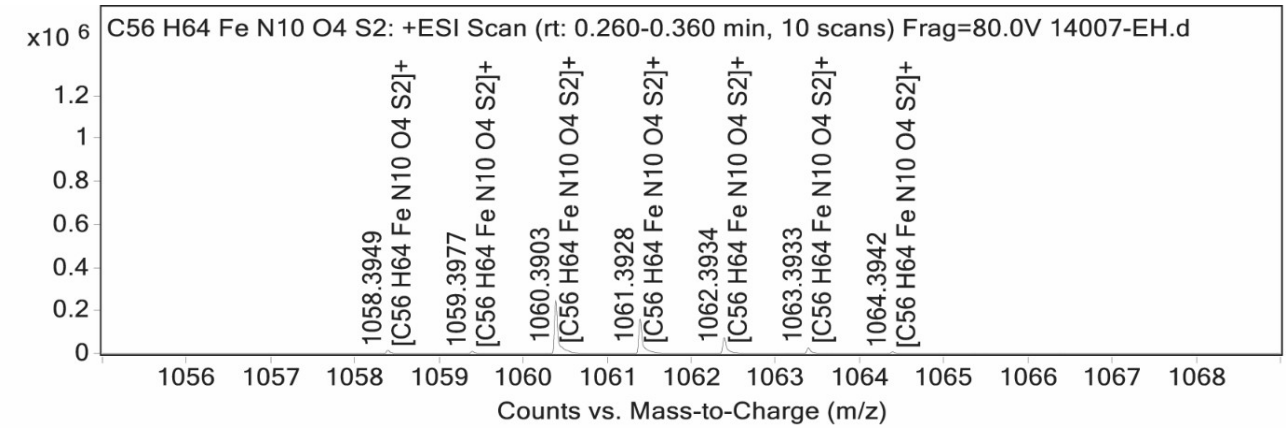

Figure S9. HR-ESI (positive ions) mass spectrum of **$FeSO_2$**.

NMR spectroscopy data

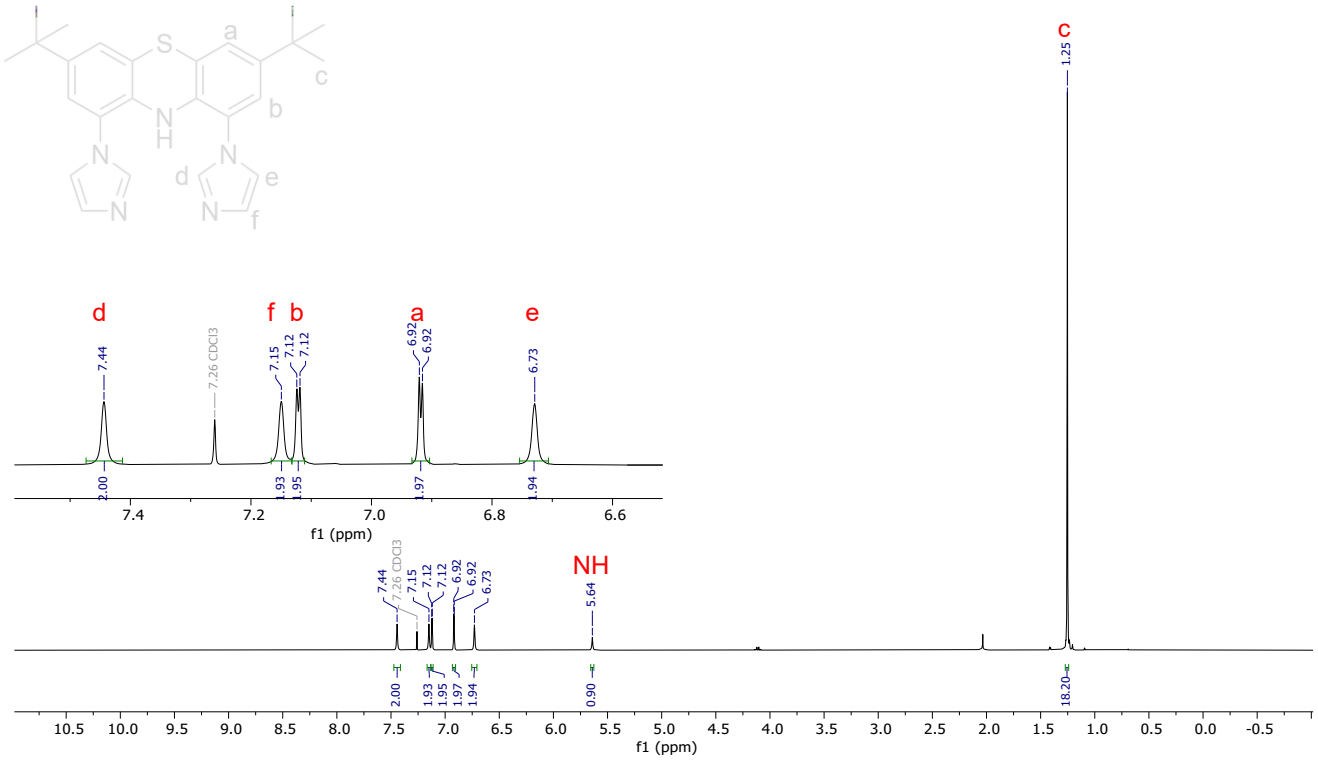

Figure S10. ^{1}H NMR spectrum of **4** (600 MHz, $CDCl_3$).

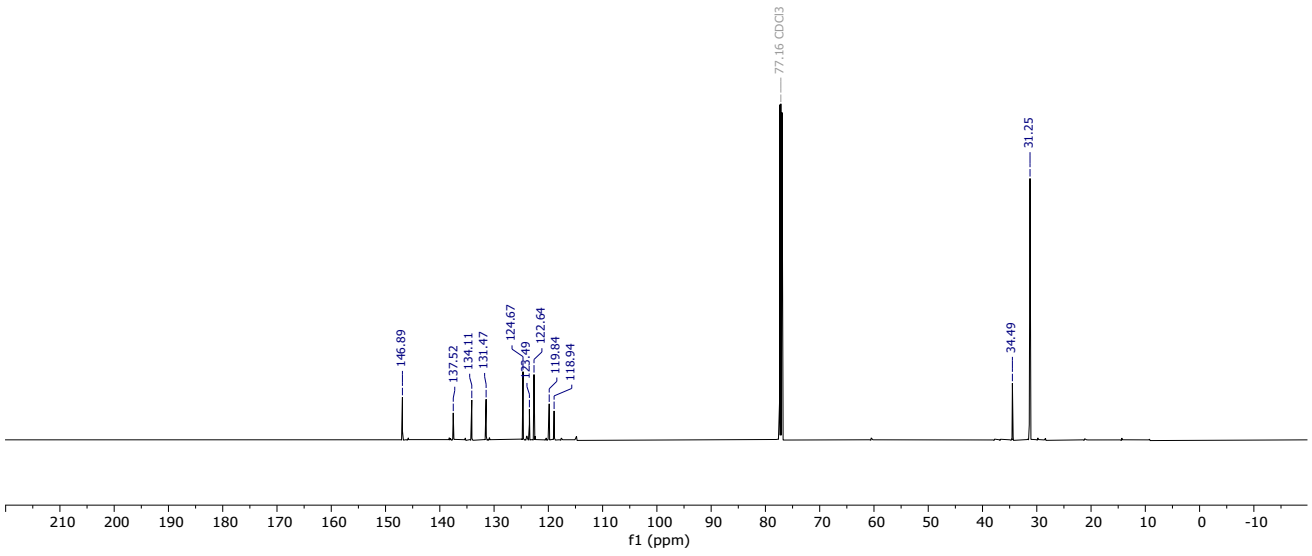

Figure S11. $^{13}C\{^{1}H\}$ NMR spectrum of **4** (151 MHz, $CDCl_3$).

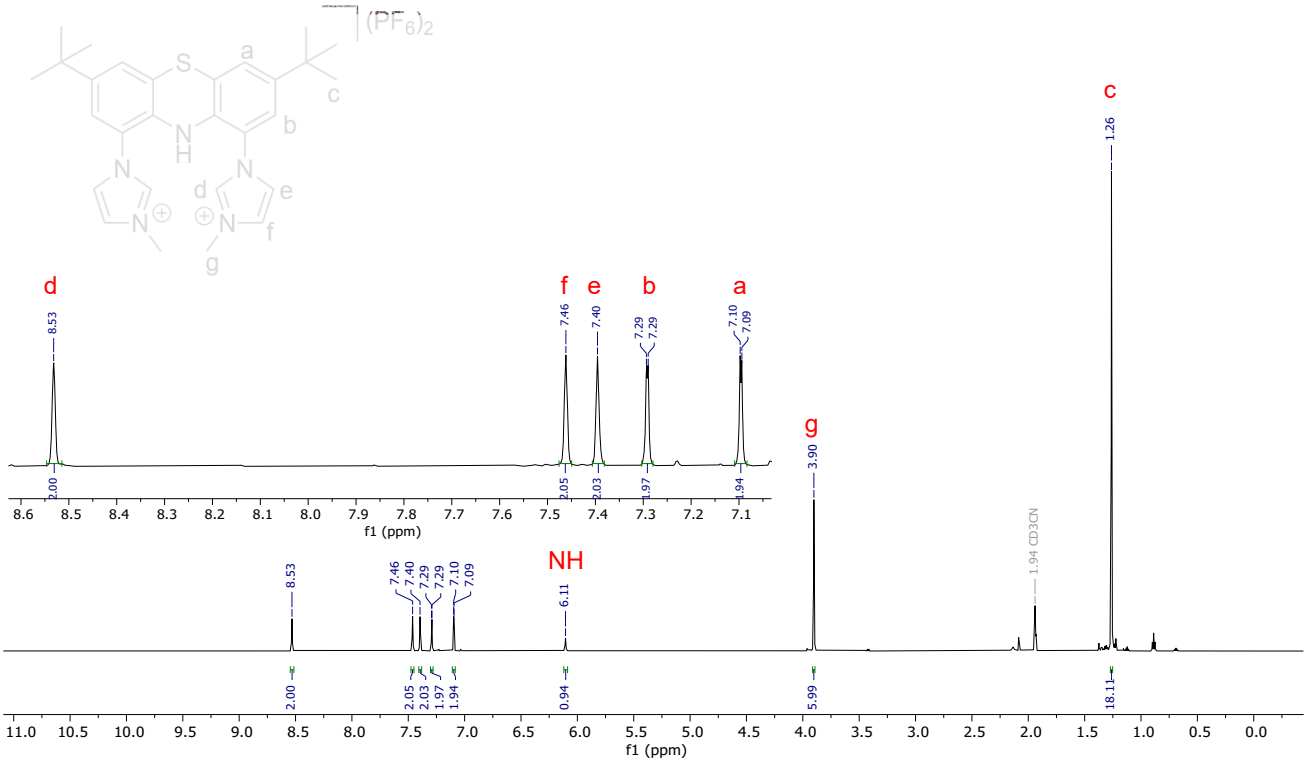

Figure S12. ^{1}H NMR spectrum of **PTZIm$_2$H** (600 MHz, CD_3CN).

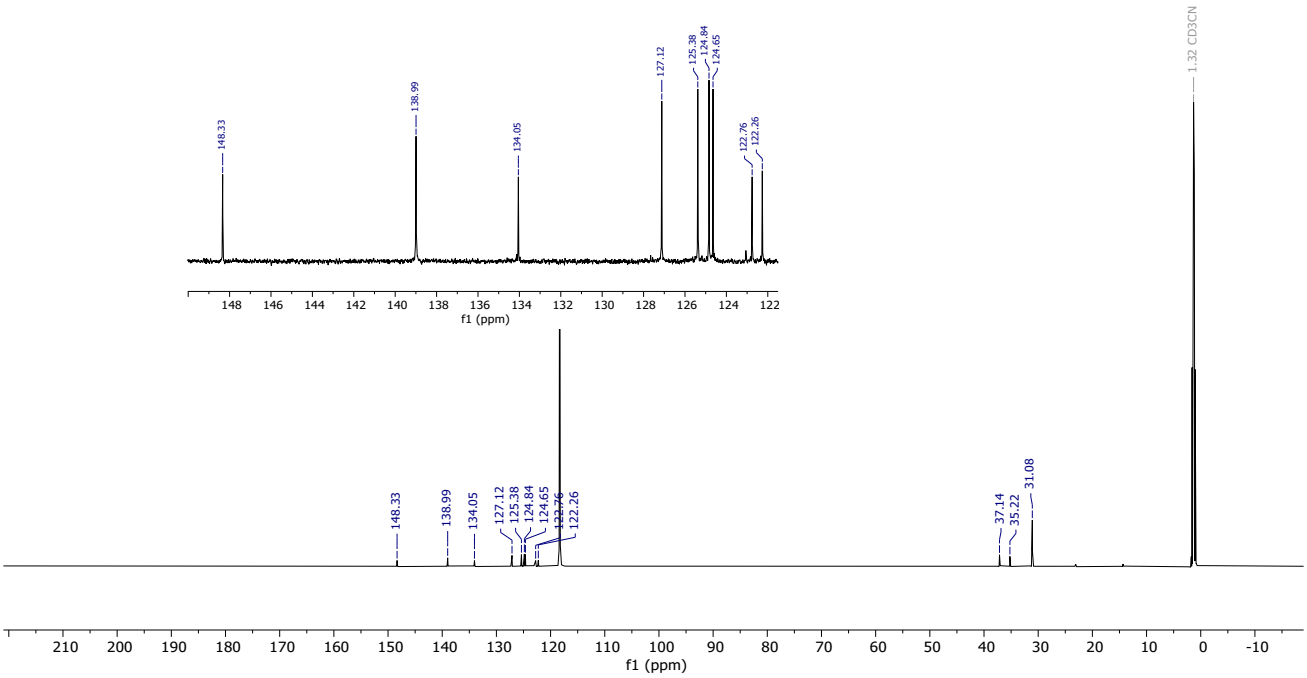

Figure S13. $^{13}C\{^{1}H\}$ NMR spectrum of **PTZIm$_2$H** (151 MHz, CD_3CN).

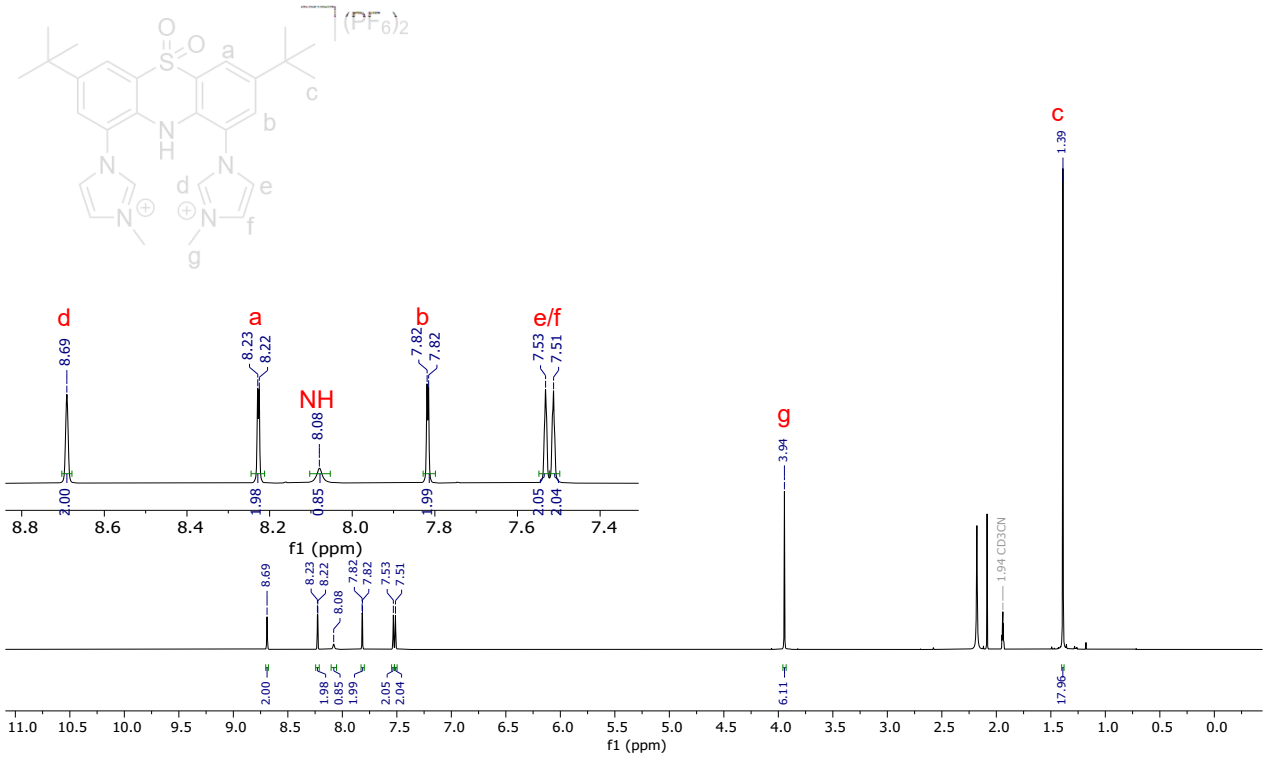

Figure S14. ^{1}H NMR spectrum of **$PTZO_2Im_2H$** (600 MHz, CD_3CN).

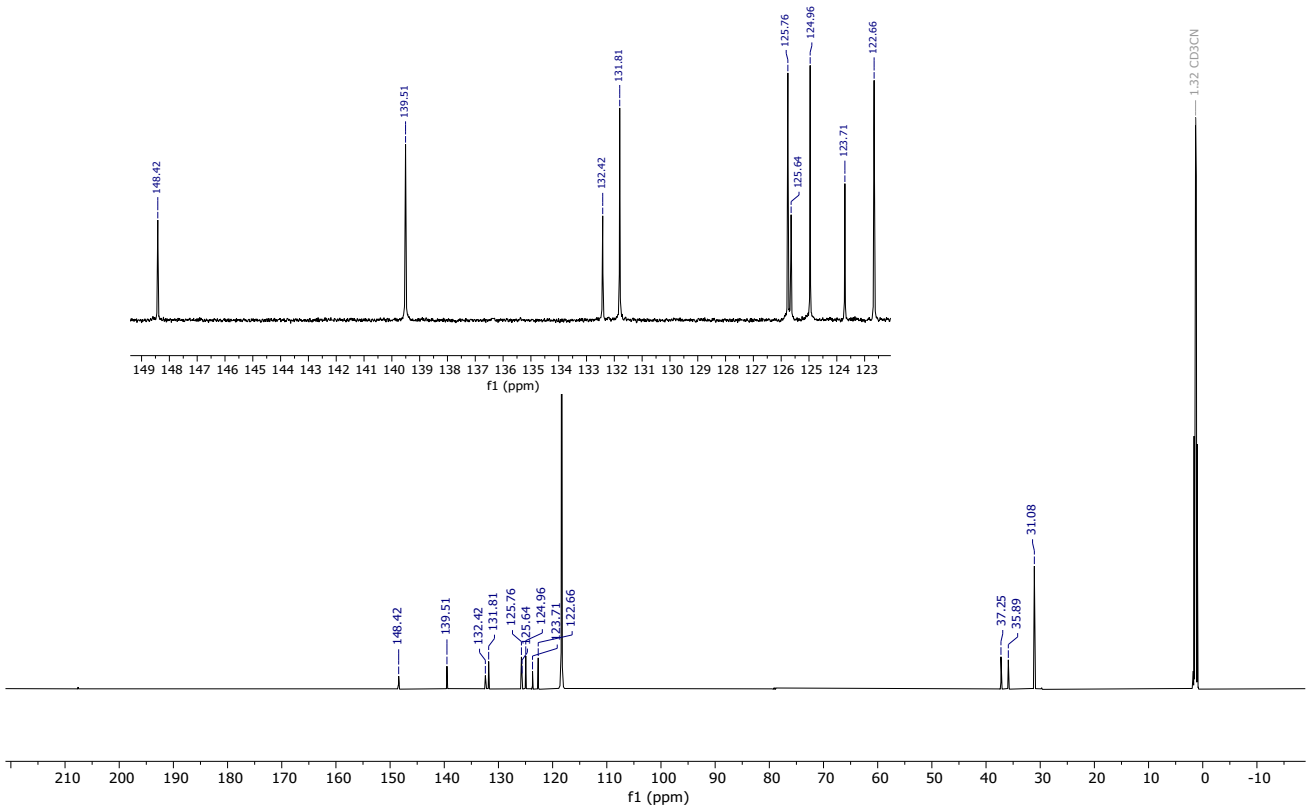

Figure S15. $^{13}C\{^{1}H\}$ NMR spectrum of **$PTZO_2Im_2H$** (151 MHz, CD_3CN).

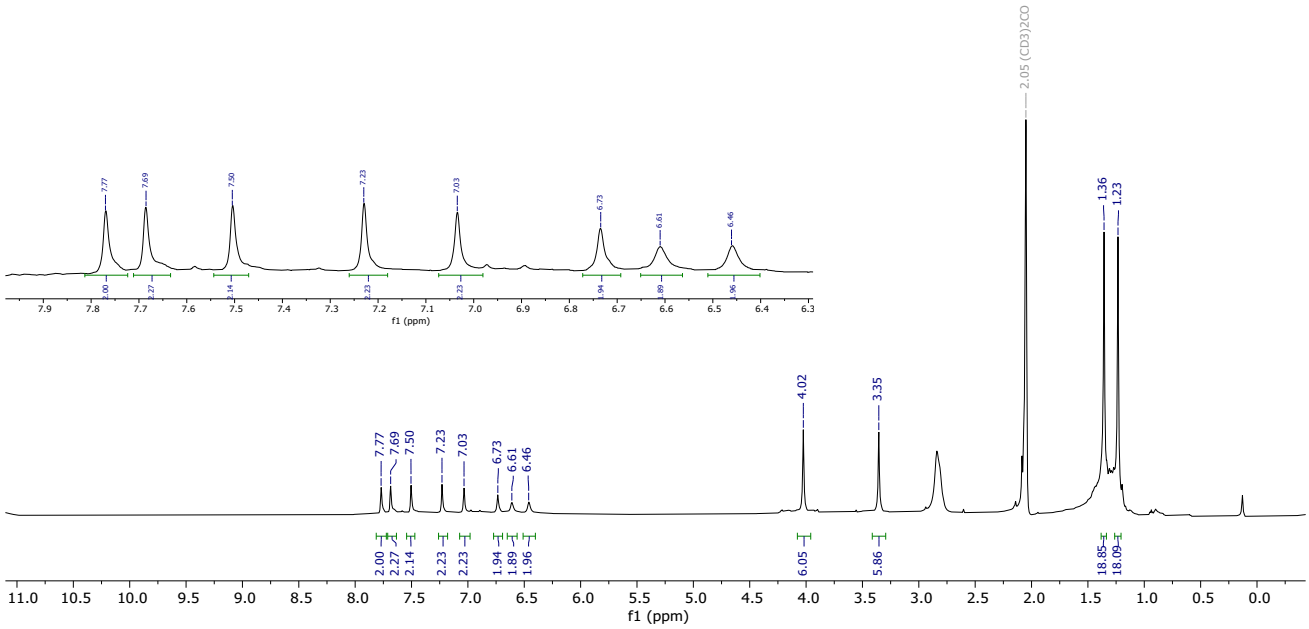

Figure S16. ^{1}H NMR spectrum of **CoS** (600 MHz, Acetone-d_6).

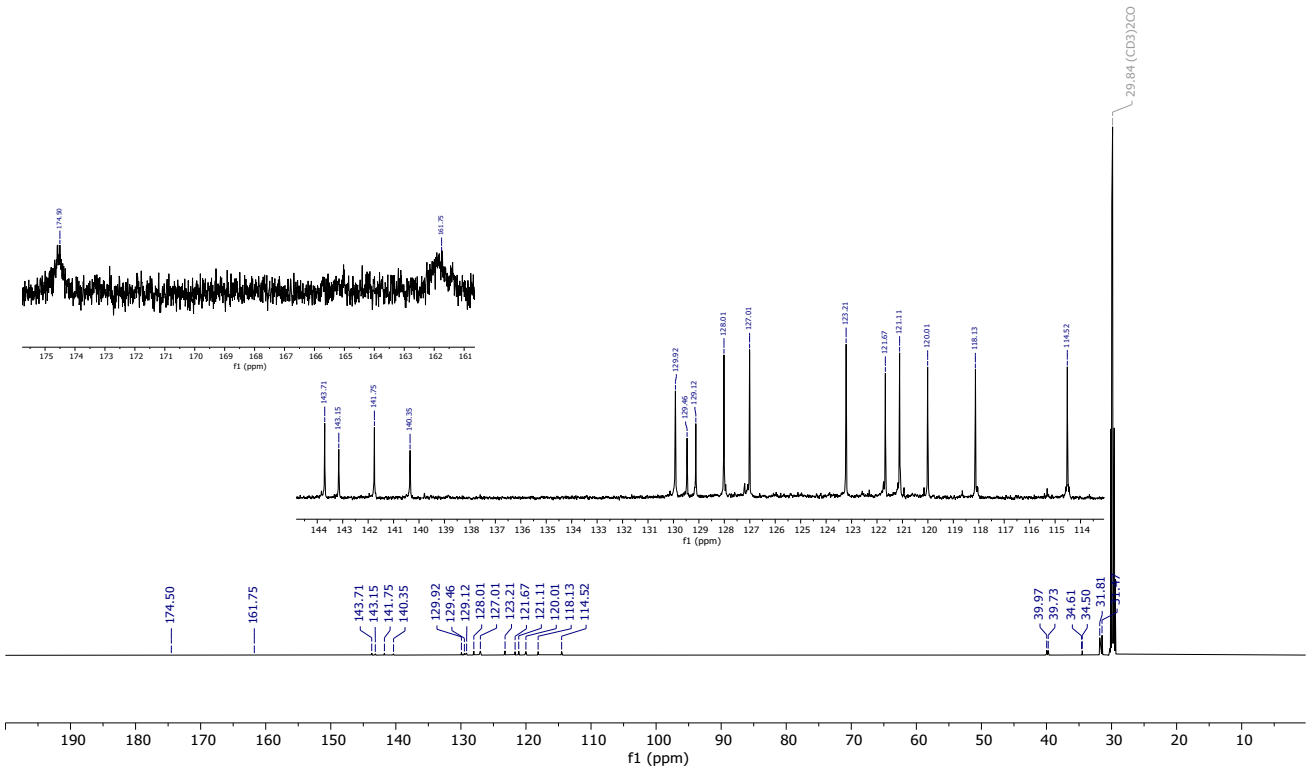

Figure S17. $^{13}C\{^{1}H\}$ NMR spectrum of **CoS** (151 MHz, Acetone-d_6).

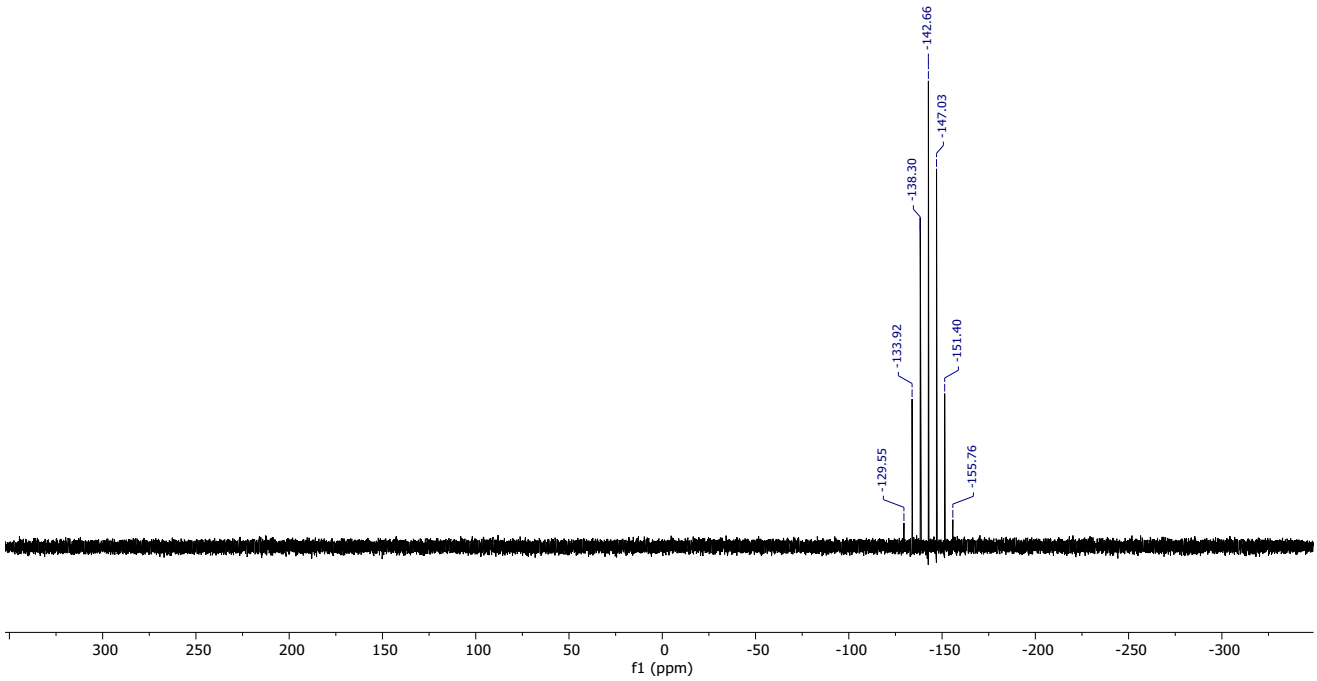

Figure S18. $^{31}P\{^{1}H\}$ NMR spectrum of **CoS** (162 MHz, Acetone-d_6).

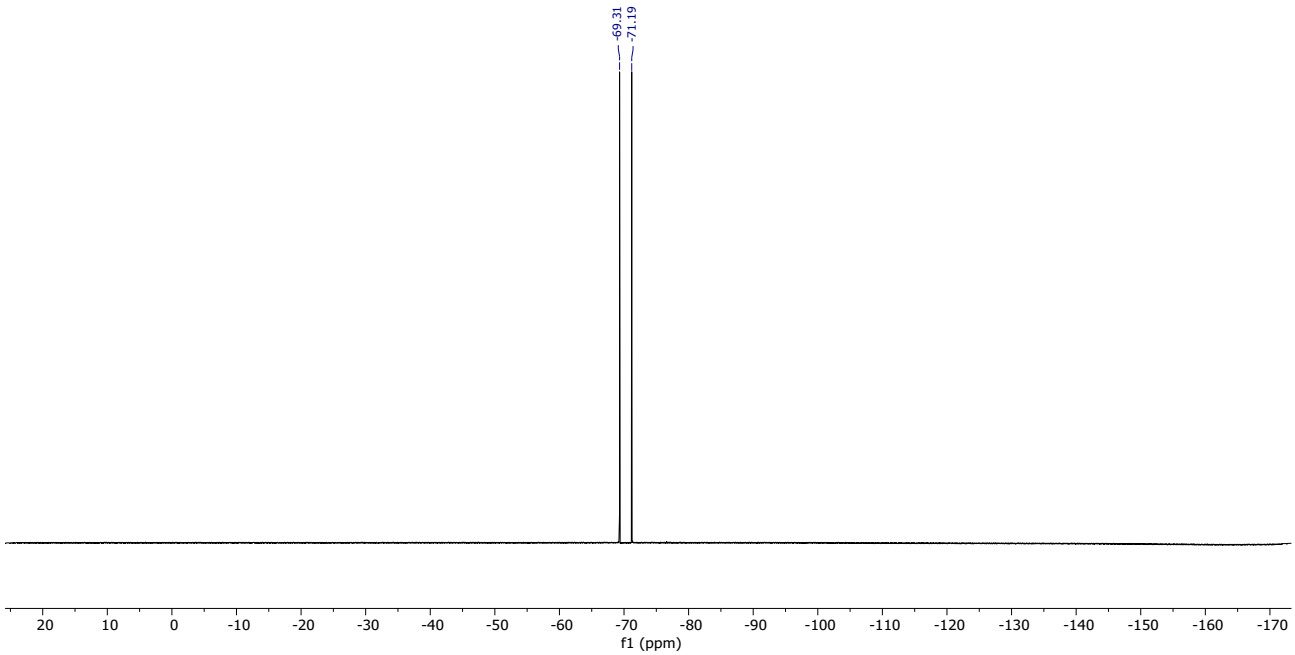

Figure S19. $^{19}F\{^{1}H\}$ NMR spectrum of **CoS** (377 MHz, Acetone-d_6).

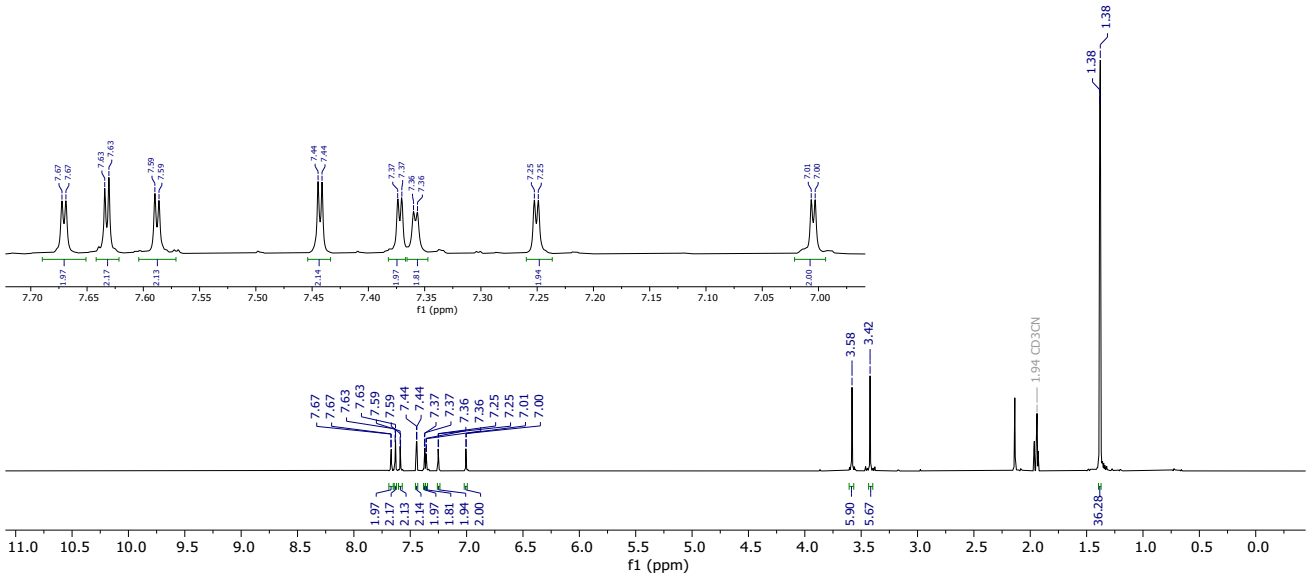

Figure S20. ^{1}H NMR spectrum of **$CoSO_2$** (600 MHz, CD_3CN).

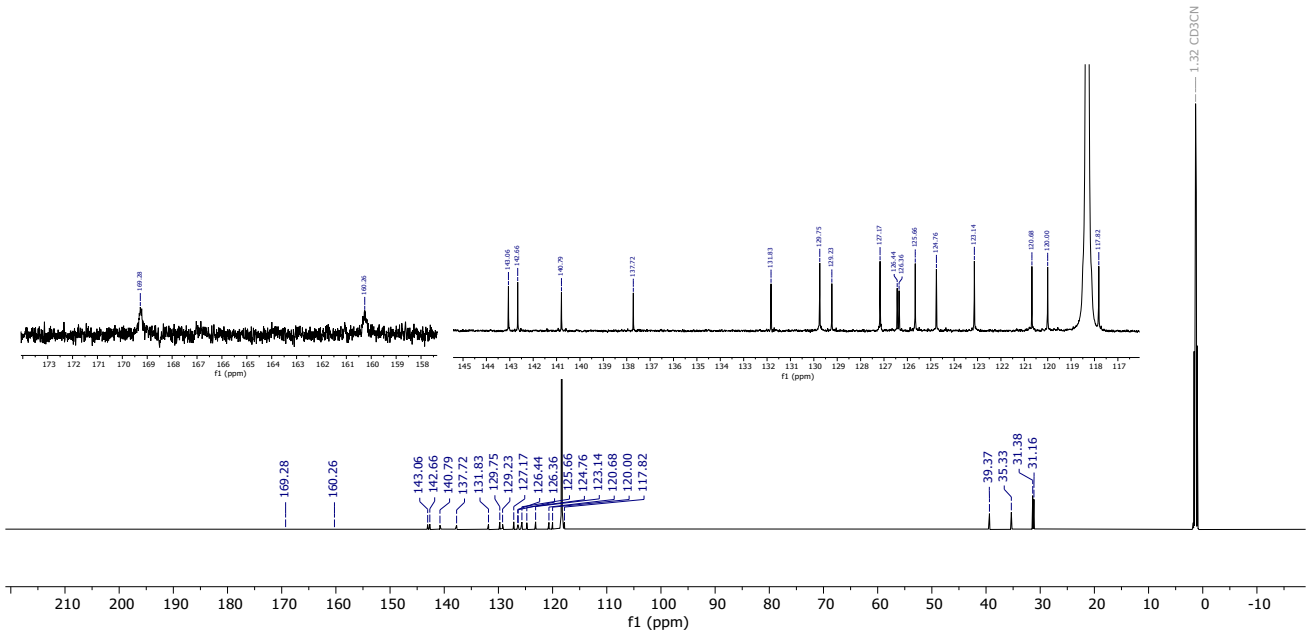

Figure S21. $^{13}C\{^{1}H\}$ NMR spectrum of **$CoSO_2$** (151 MHz, CD_3CN).

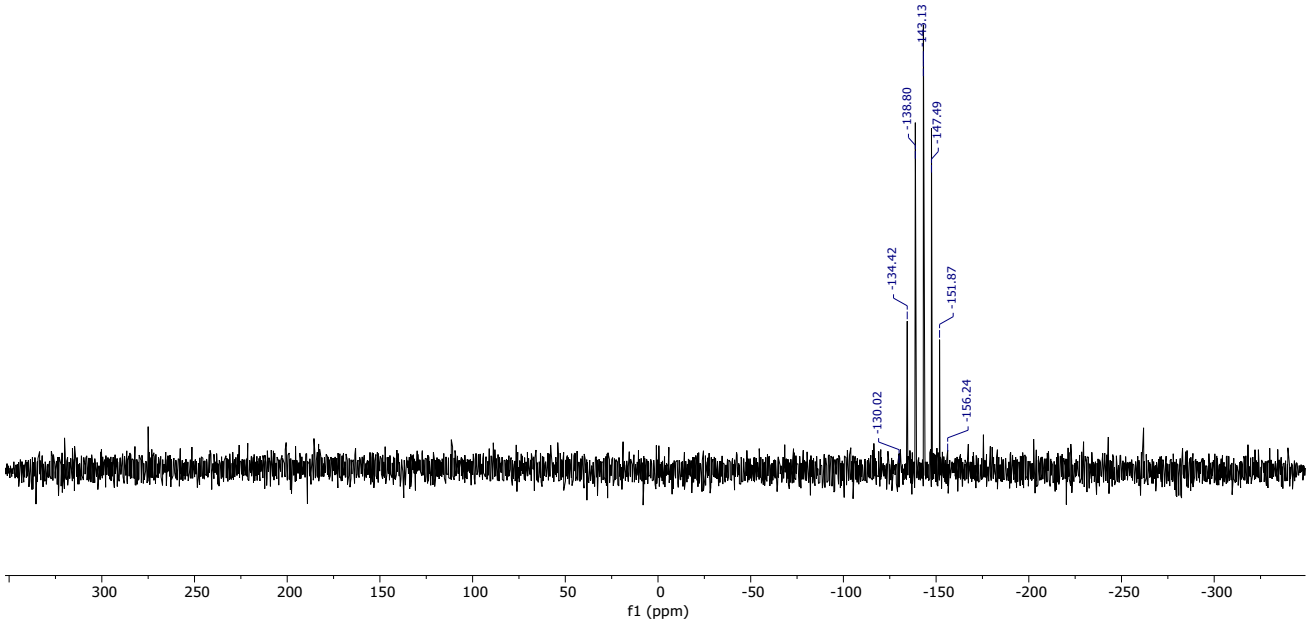

Figure S22. $^{31}P\{^{1}H\}$ NMR spectrum of **$CoSO_2$** (162 MHz, CD_3CN).

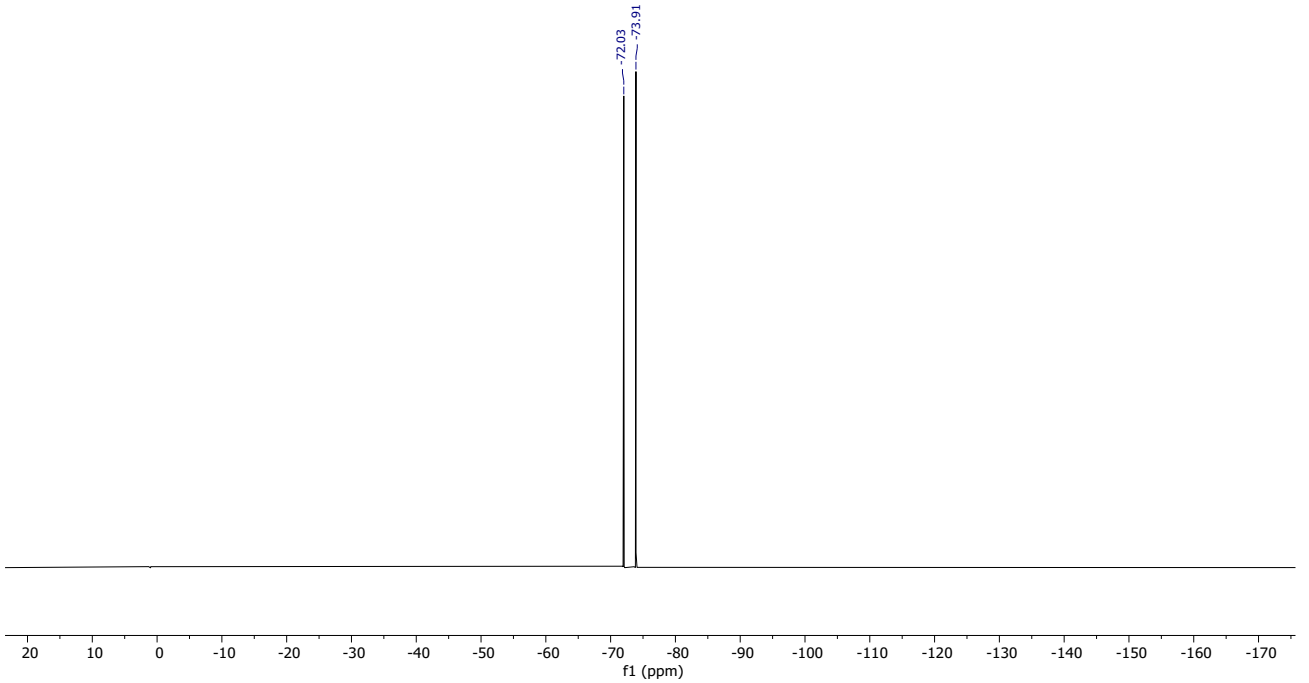

Figure S23. $^{19}F\{^{1}H\}$ NMR spectrum of **$CoSO_2$** (377 MHz, CD_3CN).

EPR spectroscopy data

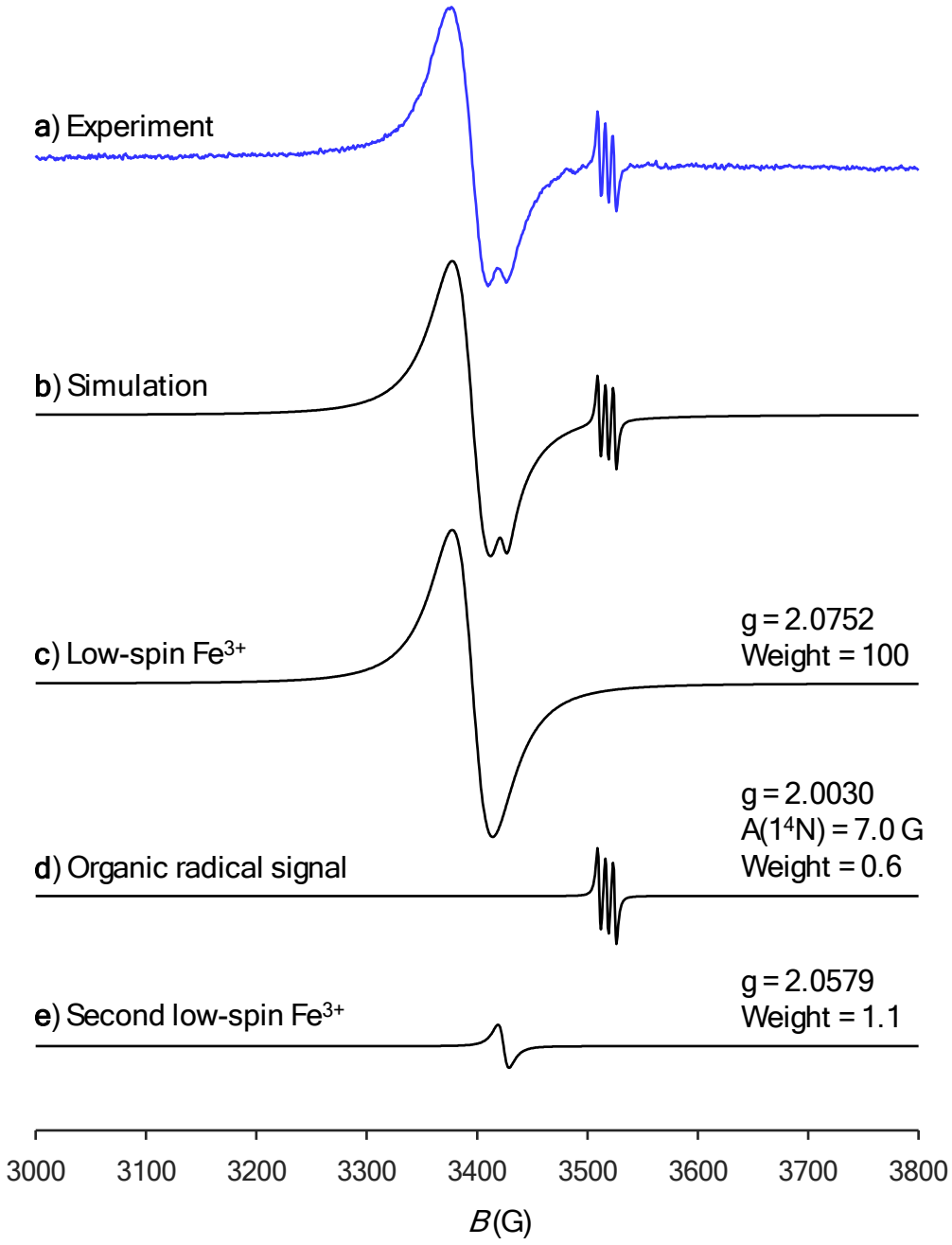

Figure S24. Room-temperature EPR spectra in acetonitrile of **FeS** in acetonitrile, and spectral simulation. (**a**) Experimental spectrum, (**b**) Simulated spectrum from weighted sum of three components, (**c**) Component 1: low-spin Fe(III) species (**d**), Component 2: organic radical (**e**), Component 3: second low-spin Fe(III) species. *Experimental parameters:* microwave frequency = 9.8622 MHz, microwave power = 20 mW, modulation amplitude = 8 Gauss, sweep time = 20 s, time constant = 2.48 ms, number of scans = 20.

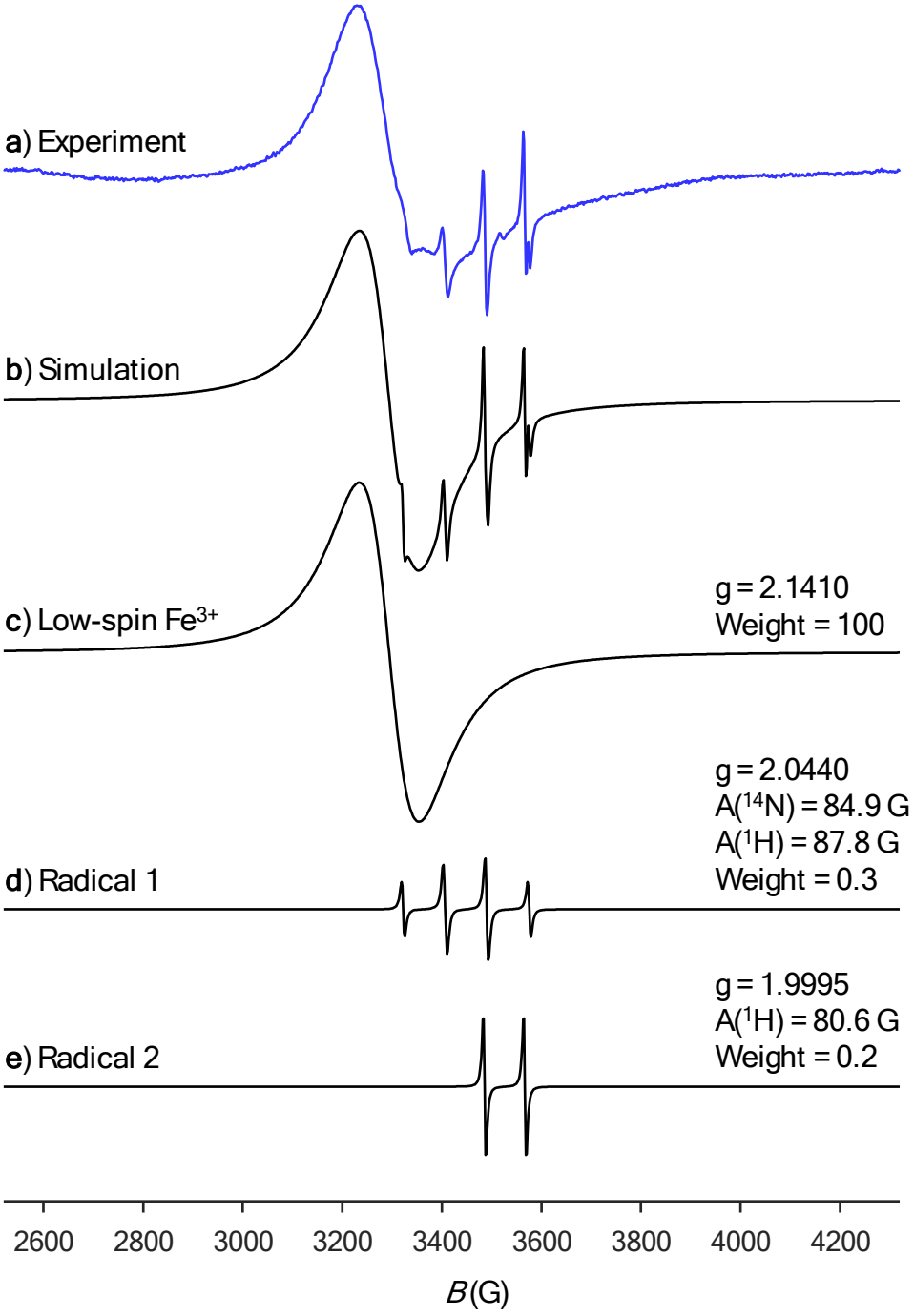

Figure S25. Room-temperature EPR spectra in acetonitrile of **$FeSO_2$** in acetonitrile, and spectral simulation. (**a**) Experimental spectrum, (**b**) Simulated spectrum from weighted sum of three components, (**c**) Component 1: low-spin Fe(III) species (**d**), Component 2: organic radical, (**e**) Component 3: second organic radical. *Experimental parameters:* microwave frequency = 9.8617 MHz, microwave power = 20 mW, modulation amplitude = 8 Gauss, sweep time = 30 s, time constant = 2.48 ms, number of scans = 100.

XRD data

Table S1. Crystal and structure determination data for complex **$CoSO_2$**.

Formula	$C_{56}H_{64}CoN_{10}O_4S_2F_6P \bullet 1.351(CH_2Cl_2)$
Molecular weight	1324.02
T / K	100
a / Å	12.9740(8)
b / Å	13.7037(9)
c / Å	17.0534(12)
α / deg	96.409(2)
β / deg	90.190(2)
γ / deg	99.233(2)
V/ Å^3	2973.3(3)
Crystal color	Orange
Crystal system	Triclinic
Space group	P$\bar{1}$
Z	2
F(000)	1374
D_c / gcm^{-3}	1.479
Crystal dimensions / mm	0.27 × 0.16 × 0.11
λ / Å	0.71073
μ / mm^{-1}	0.582
Collection range	$1.202 \leq \theta \leq 23.371°$ (*h*: −11 to 14; *k*: −15 to 14; *l*: −19 to 18)
Completeness to theta	0.993
No. of data collected	28119
No. of unique data	8607
No. of data used in refinement, *m*	5744
No. of parameters refined, *p*	792
R^a	0.0710
wR^a	0.1771
Goodness-of-fit, S	1.033
Maximum shift, $(\Delta/\sigma)_{max}$	0.000
Residual extrema in final difference map, eÅ^{-3}	+0.918, –0.803

Table S2. Crystal and structure determination data for complex **$FeSO_2$**.

Formula	$C_{56}H_{64}FeN_{10}O_4S_2F_6P \bullet 2(CH_2Cl_2)$
Molecular weight	1375.96
T / K	100
a / Å	13.0694(6)
b / Å	13.8108(6)
c / Å	17.0915(7)
α / deg	83.078(2)
β / deg	88.626(2)
γ / deg	80.133(2)
V/ Å^3	3017.2(2)
Crystal color	Green/Yellow
Crystal system	Triclinic
Space group	$P\bar{1}$
Z	2
F(000)	1426
D_c / gcm^{-3}	1.515
Crystal dimensions / mm	0.16 × 0.13 × 0.07
λ / Å	0.71073
μ / mm^{-1}	0.598
Collection range	$1.200 \leq \theta \leq 28.489°$ (h: −17 to 17; k: −18 to 18; l: −18 to 22)
Completeness to theta	99.1%
No. of data collected	80048
No. of unique data	15167
No. of data used in refinement, m	10927
No. of parameters refined, p	791
R^a	0.0547
wR^a	0.1342
Goodness-of-fit, S	1.018
Maximum shift, $(\Delta/\sigma)_{max}$	0.001
Residual extrema in final difference map, eÅ^{-3}	+1.496, −1.117

Table S3. Selected bond distances (Å) and angles (°) with estimated standard deviations (e.s.d.s.) in parentheses for **$CoSO_2$** and **$FeSO_2$**.

		Selected bond lengths (Å)		
$CoSO_2$	Co(1)–N(3)	2.065(5)	Co(1)–C(27)	1.925(7)
	Co(1)–N(8)	2.025(5)	Co(1)–C(30)	1.950(6)
	Co(1)–C(2)	1.974(6)	Co(1)–C(55)	2.014(6)
$FeSO_2$	Fe(1)–N(3)	1.996(2)	Fe(1)–C(27)	1.982(3)
	Fe(1)–N(8)	2.056(2)	Fe(1)–C(30)	1.987(3)
	Fe(1)–C(2)	2.050(3)	Fe(1)–C(55)	2.000(3)
		Selected bond angles (°)		
$CoSO_2$	N(3)–Co(1)–C(2)	89.9(2)	N(8)–Co(1)–C(30)	89.1(2)
	N(3)–Co(1)–C(27)	78.4(2)	N(8)–Co(1)–C(55)	83.0(2)
	N(3)–Co(1)–C(30)	175.5(2)	N(8)–Co(1)–C(27)	172.7(2)
$FeSO_2$	N(3)–Fe(1)–C(2)	83.54(10)	N(8)– Fe(1)–C(30)	79.24(10)
	N(3)–Fe(1)–C(27)	89.84(11)	N(8)–Fe(1)–C(55)	89.80(10)
	N(3)–Fe(1)–C(30)	173.26(10)	N(8)–Fe(1)–C(27)	175.65(11)

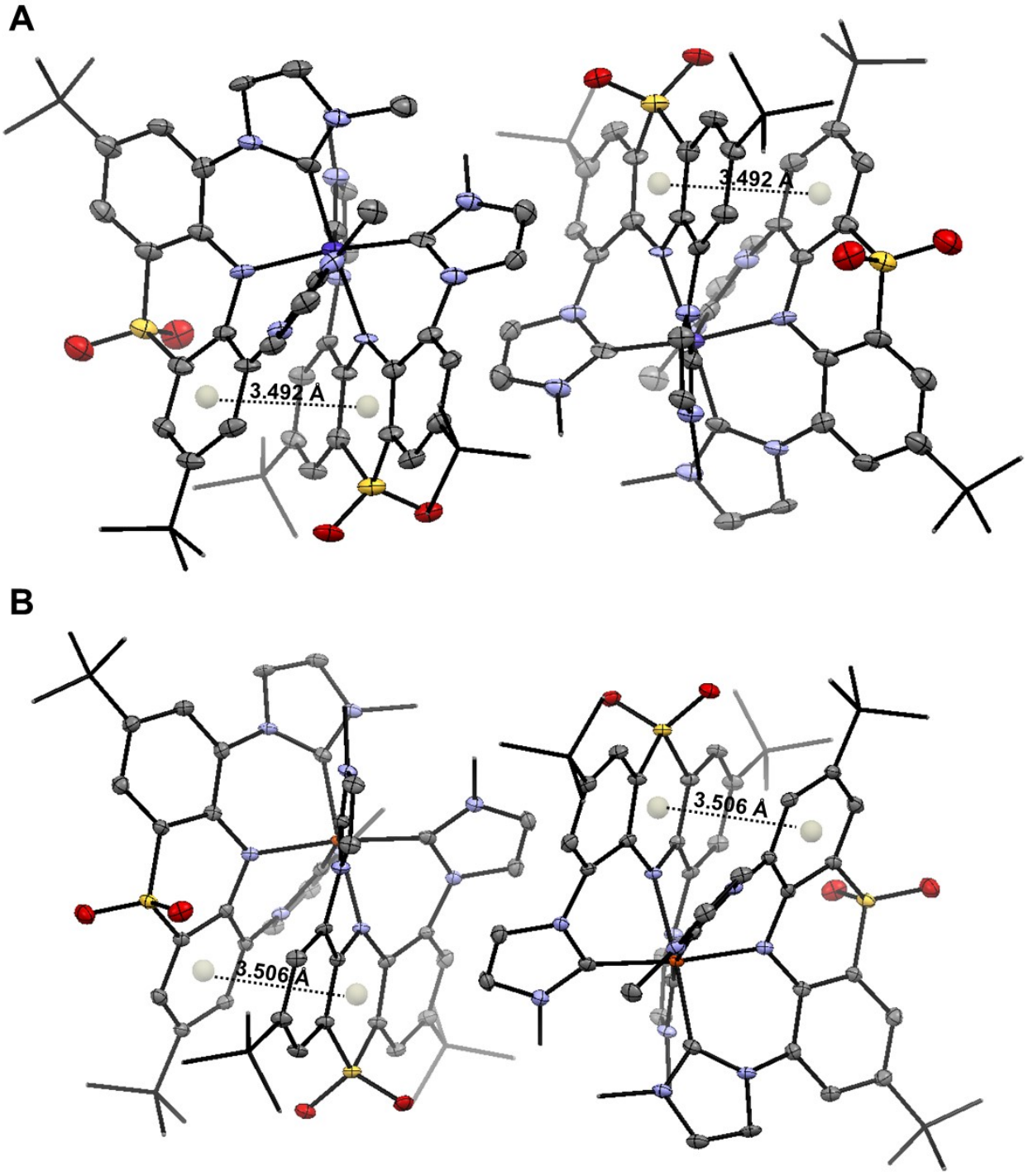

Figure S26. Molecular packing of complexes **$CoSO_2$** (A) and **$FeSO_2$** (B) showing π-π interactions, relevant centroids and the distances between them are shown. Hydrogen atoms, counter ions and solvent molecules are omitted for clarity. Thermal ellipsoids at 50% probability.

.

Ground-state and emission spectroscopy data

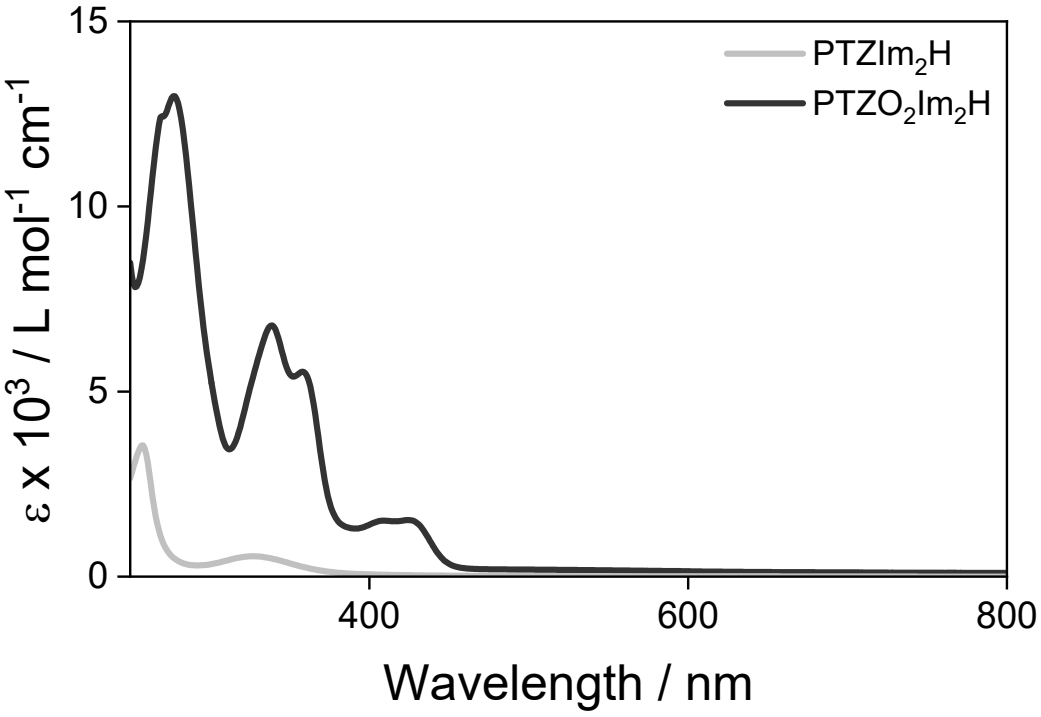

Figure S27. UV-vis absorption spectrum of **$PTZIm_2H$** and **$PTZO_2Im_2H$** at 298 K in acetonitrile.

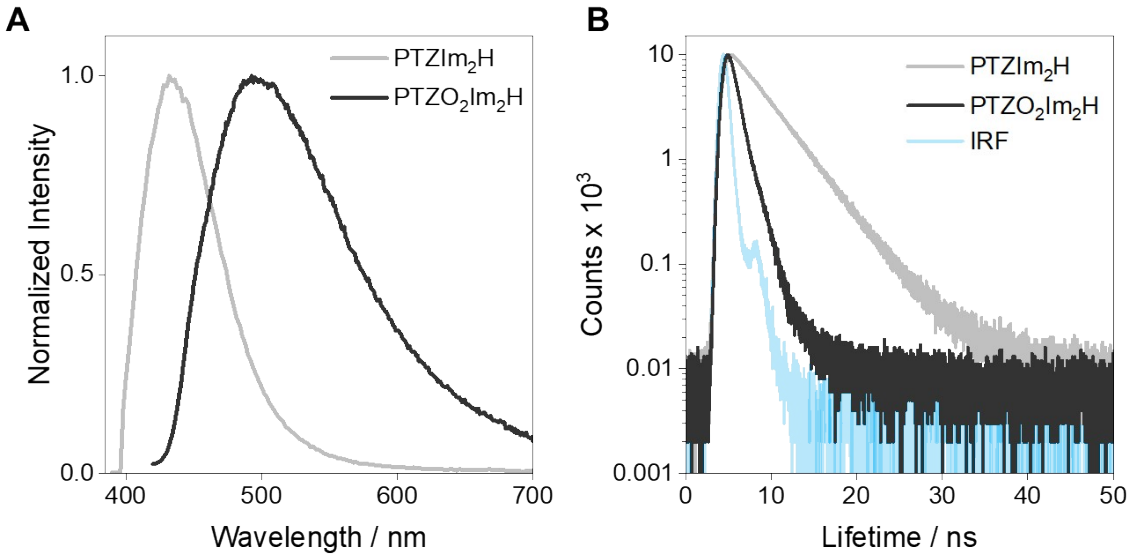

Figure S28. Photoluminescence spectra of **$PTZIm_2H$** and **$PTZO_2Im_2H$** at 298 K in acetonitrile (A) Emission decay of **$PTZIm_2H$** and **$PTZO_2Im_2H$** in acetonitrile at 298 K (B).

Table S4. Photoluminescence data of ligands **$PTZIm_2H$** and **$PTZO_2Im_2H$** in acetonitrile at 298 K.

Compound	Emission λ_{em} / nm	τ_{em} / ns	Φ_{em}
$PTZIm_2H$	432	4.0 ns	0.9%
$PTZO_2Im_2H$	493	0.9 ns (99%) + 6.9 ns (1%)	1.3%

Computational data

Table S5. Selected bond lengths (Å), bond angles (°) at optimized S_0 geometry for complexes $CoSO_2$ using B3LYP/ZORA-def2-TZVP(-f).

Bond	S_0 DFT	XRD	Error / %
Selected bond lengths (Å)			
Co(1)–N(3)	2.07808	2.0655	0.61%
Co(1)–N(8)	2.00434	2.0255	1.04%
Co(1)–C(27)	1.9604	1.9257	1.80%
Co(1)–C(30)	1.972	1.9506	1.10%
Co(1)–C(2)	1.97739	1.9746	0.14%
Co(1)–C(55)	2.04786	2.0146	1.65%
Selected bond angles (°)			
N(3)–Co(1)–C(2)	89.316	89.92	0.67%
N(3)–Co(1)–C(27)	77.865	78.42	0.71%
N(3)–Co(1)–C(30)	170.222	175.52	3.02%
N(8)–Co(1)–C(30)	88.597	89.12	0.59%
N(8)–Co(1)–C(55)	81.613	83.02	1.69%
N(8)–Co(1)–C(27)	174.566	172.72	1.07%
C(55)–Co(1)–C(2)	163.186	168.91	3.39%

Table S6. Selected bond lengths (Å), bond angles (°) at optimized T_1 and S_0 geometry of complexes **CoS** and **$CoSO_2$** within B3LYP/def2-TZVP(-F) level of theory and the root-mean-square deviation (RMSD) comparing the optimized T_1 and S_0 geometries.

	CoS		**$CoSO_2$**	
	T_1	S_0	T_1	S_0
Selected bond lengths (Å)				
Co(1)–N(3)	2.26191	2.00967	2.27606	2.07808
Co(1)–N(8)	2.11280	2.01234	1.93486	2.00434
Co(1)–C(27)	2.04339	1.99534	2.00540	1.96040
Co(1)–C(30)	2.16995	1.99724	2.34893	1.97200
Co(1)–C(2)	1.98539	2.01764	2.01725	1.97739
Co(1)–C(55)	1.96605	2.01145	2.02957	2.04786
Selected bond angles (º)				
N(3)–Co(1)–C(30)	162.105	168.426	167.814	170.222
N(8)–Co(1)–C(27)	160.672	168.504	179.679	174.566
C(55)–Co(1)–C(2)	178.121	179.193	162.937	163.186
RMSD	0.333		0.314	

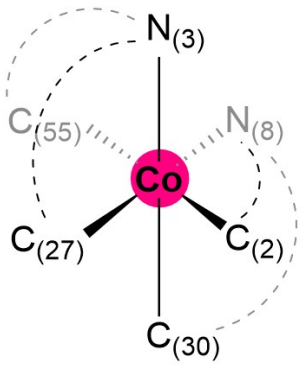

Table S7. First and selected singlet excited states of complex **CoS** (f > 0.05) with oscillator strength calculated by TD-DFT at optimized geometries.

Complex	S_n[a]	Excitation (contribution)[b]	Vertical excitation energy		Oscillator strength (f)
			eV	nm	
CoS	S_1	H−1 → L (0.57)	2.16	575	0.0005
	S_4	H → L+1 (0.82)	2.72	456	0.0677
	S_{10}	H → L+4 (0.20) H → L+3 (0.11) H−1 → L+3 (0.11)	3.17	391	0.0726
	S_{11}	H−1 → L+3 (0.19) H → L+5 (0.19) H → L+4 (0.18)	3.17	391	0.0547
	S_{14}	H−1 → L+4 (0.27) H → L+2 (0.18)	3.27	380	0.0766
	S_{19}	H−1 → L+7 (0.64)	3.47	357	0.0814
	S_{35}	H−2 → L+3 (0.66) H−1 → L+11 (0.10)	4.38	283	0.0670
	S_{38}	H−2 → L+2 (0.38) H → L+12 (0.35)	4.42	280	0.1897

[a] Vertical states taking S_0 geometry as the reference; [b] Transitions with a percentage higher than 10% are shown in parenthesis.

Table S8. First and selected singlet excited states of complex **$CoSO_2$** (f > 0.05) with oscillator strength calculated by TD-DFT at optimized geometries.

Complex	S_n[a]	Excitation (contribution)[b]	Vertical excitation energy		Oscillator strength (f)
			eV	nm	
$CoSO_2$	S_1	H−1 → L+2 (0.20) H−1 → L+1 (0.13)	2.57	482	0.0006
	S_5	H → L+1 (0.46) H → L (0.44)	3.16	393	0.0652
	S_6	H−1 → L (0.74)	3.22	385	0.0633
	S_{10}	H → L+3 (0.26) H−1 → L+2 (0.19) H−1 → L+3 (0.10)	3.48	356	0.0692
	S_{14}	H−1 → L+4 (0.72) H → L+6 (0.26)	3.76	329	0.2132
	S_{17}	H → L+7 (0.13) H−1 → L+4 (0.11) H → L+5 (0.11)	3.86	321	0.0936
	S_{19}	H → L+7 (0.65) H−2 → L+3 (0.59)	3.94	315	0.1493
	S_{28}	H−3 → L+1 (0.15) H → L+8 (0.10)	4.54	273	0.0605
	S_{39}	H−4 → L+2 (0.22) H−3 → L+2 (0.15)	4.81	258	0.0698
	S_{48}	H−2 → L+6 (0.16) H−9 → L (0.11)	4.95	251	0.0784
	S_{49}	H−7 → L+1 (0.18) H−2 → L+5 (0.16) H−5 → L+3 (0.11)	4.95	250	0.0812

[a] Vertical states taking S_0 geometry as the reference; [b] Transitions with a percentage higher than 10% are shown in parenthesis.

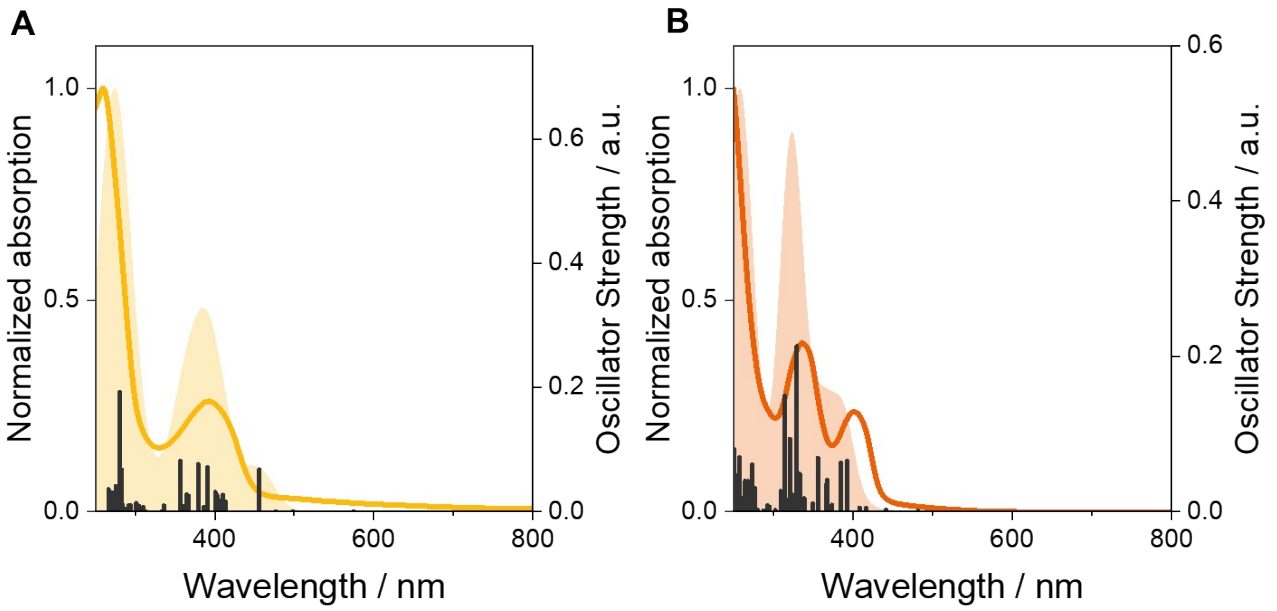

Figure S29. Experimental (solid lines) and simulated (filled curves) electronic absorption spectra for (A) **CoS** and (B) **$CoSO_2$** complexes. Transition energies and oscillator strengths calculated from TD-DFT calculations are shown by black vertical lines.

Table S9. Selected triplet excited states of complexes **CoS** and **$CoSO_2$** and oscillator strength calculated by SOC-TD-DFT at optimized geometries.

Complex	T_n[a]	Excitation (contribution)[b]	Vertical excitation energy		Oscillator strength(*f*) [c]
			eV	nm	
CoS	T_1	H−1 → L (0.35) H−1 → L+1 (0.16)	1.53	809	4.6×10^{-3}
	T_2	H−1 → L+4 (0.10) H → L (0.12)	1.98	626	1.8×10^{-3}
	T_3	H → L (0.15) H−1 → L+1 (0.14)	2.14	579	5.6×10^{-4}
$CoSO_2$	T_1	H−1 → L+2 (0.14) H−12 → L+2 (0.13)	1.83	678	2.4×10^{-3}
	T_2	H−17 → L+2 (0.10)	2.12	587	1.6×10^{-3}
	T_3	H−1 → L+3 (0.07)	2.20	565	1.6×10^{-3}
	T_4	H−14 → L+2 (0.16)	2.21	558	1.8×10^{-3}
	T_5	H−14 → L+3 (0.10)	2.55	488	3.5×10^{-4}

[a] Vertical states taking S_0 geometry as the reference; [b] Transitions with a percentage higher than 10% are shown in parenthesis; [c] *f* for the triplet states are shown as an average of the substates x, y and z. [d] Difference between states given at ground states geometry.

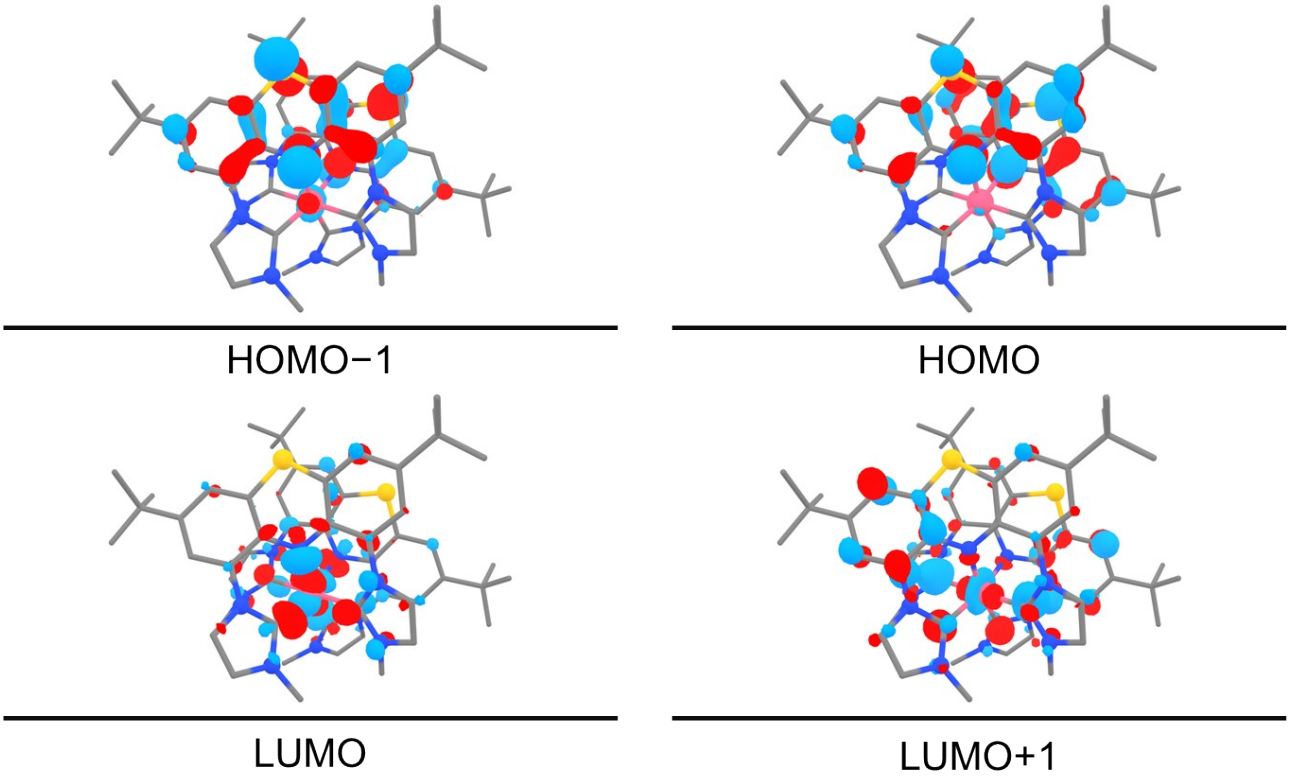

Figure S30. Ground state frontier orbitals for the complex **CoS**.

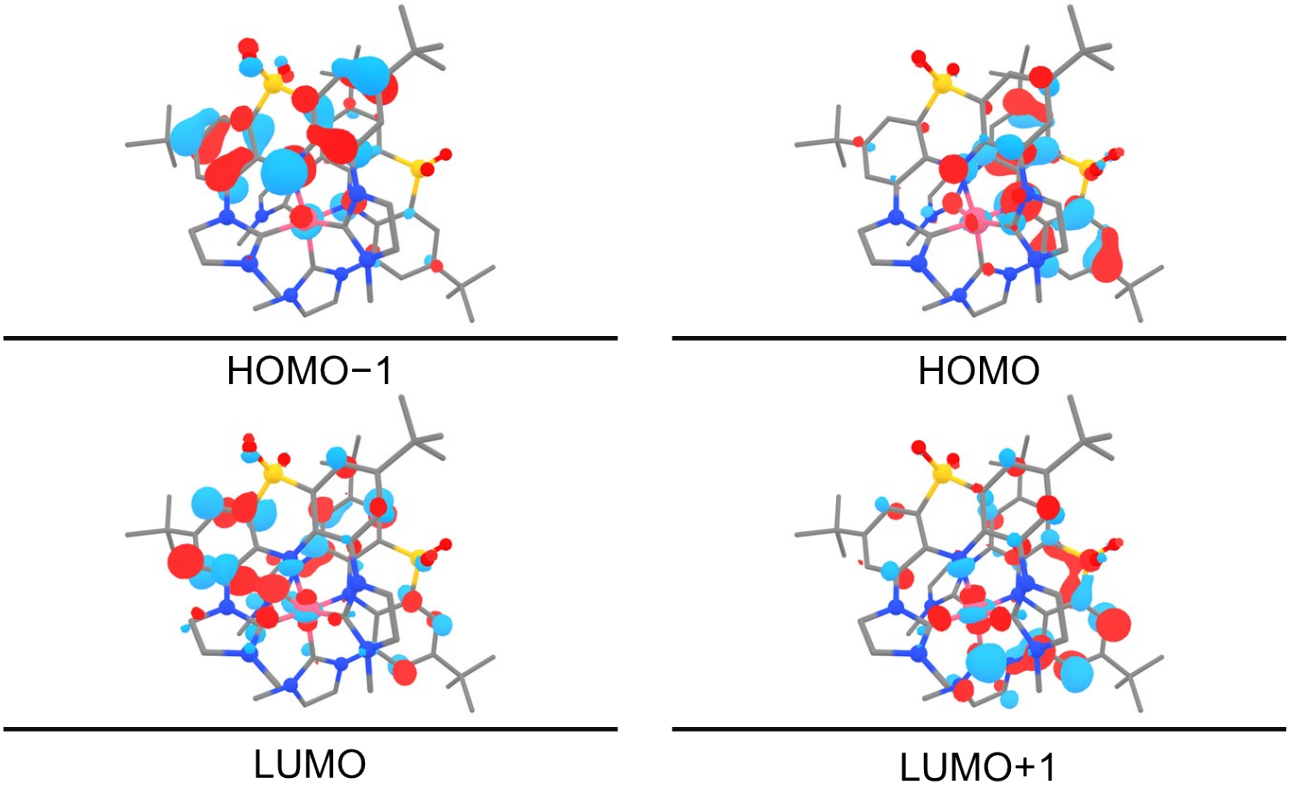

Figure S31. Ground state frontier orbitals for the complex **$CoSO_2$**.

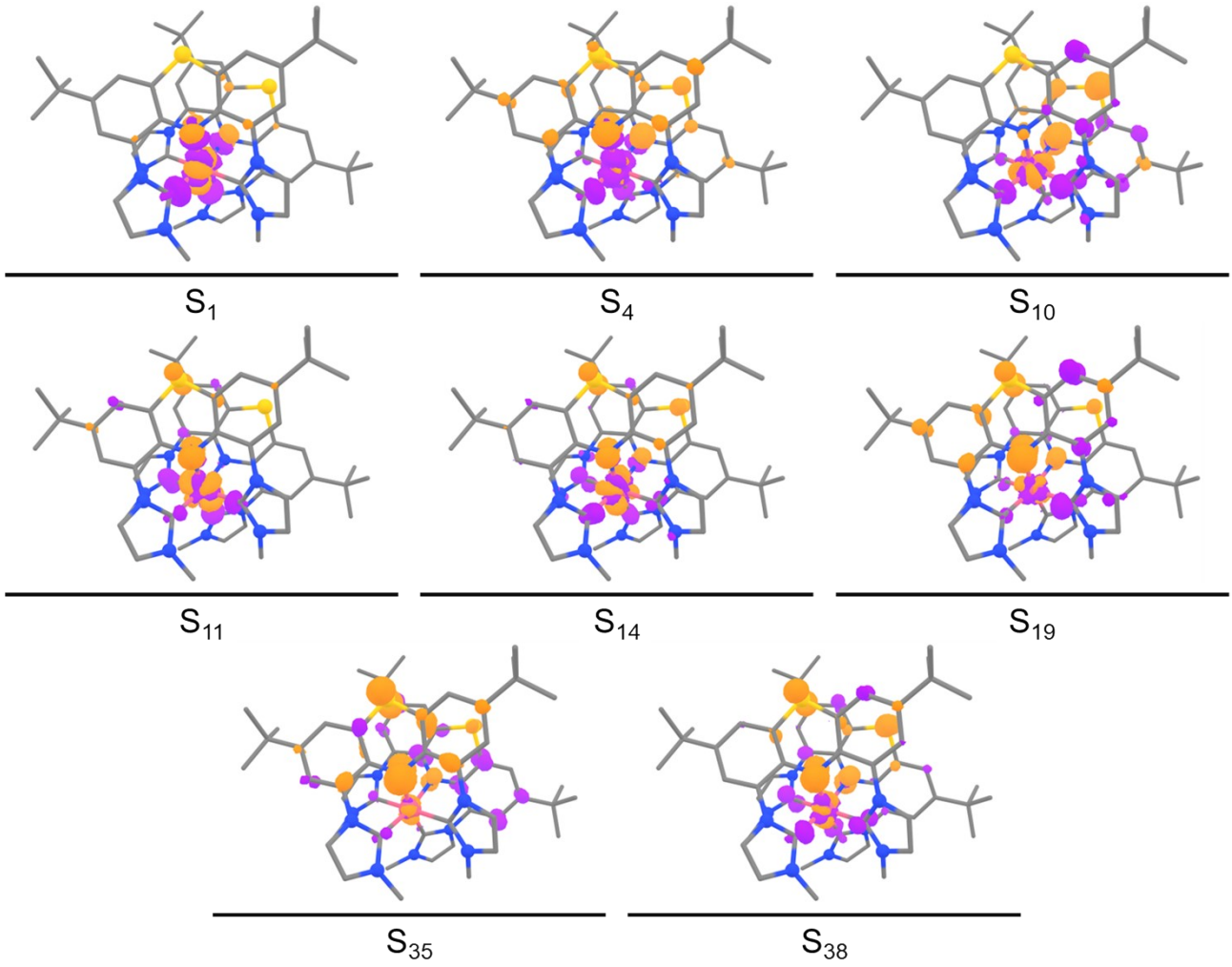

Figure S32. Electron density difference plot for S_n of **CoS** from Table S7, respectively, based on TD-DFT calculations. Orange marks a depletion, and purple indicates a gain in electron density.

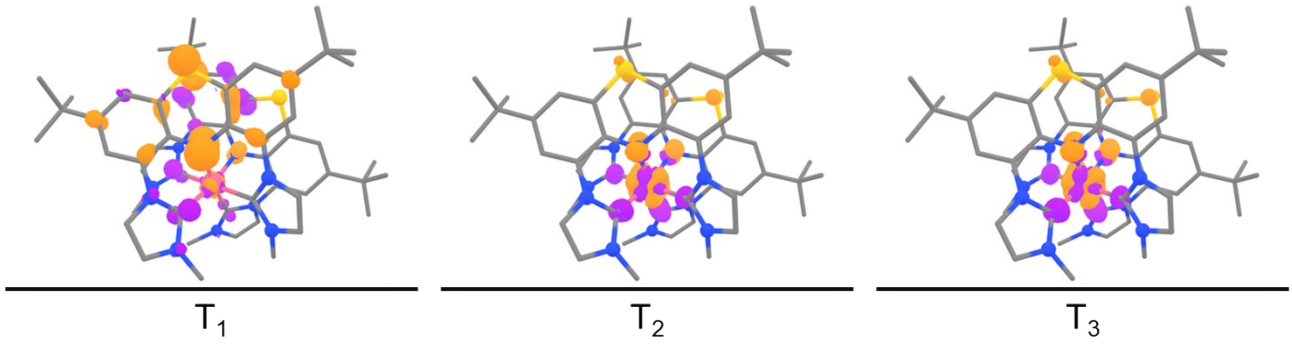

Figure S33. Electron density difference plot for T_n of **CoS** from Table S9, respectively, based on SOC-TD-DFT calculations. Orange marks a depletion, and purple indicates a gain in electron density.

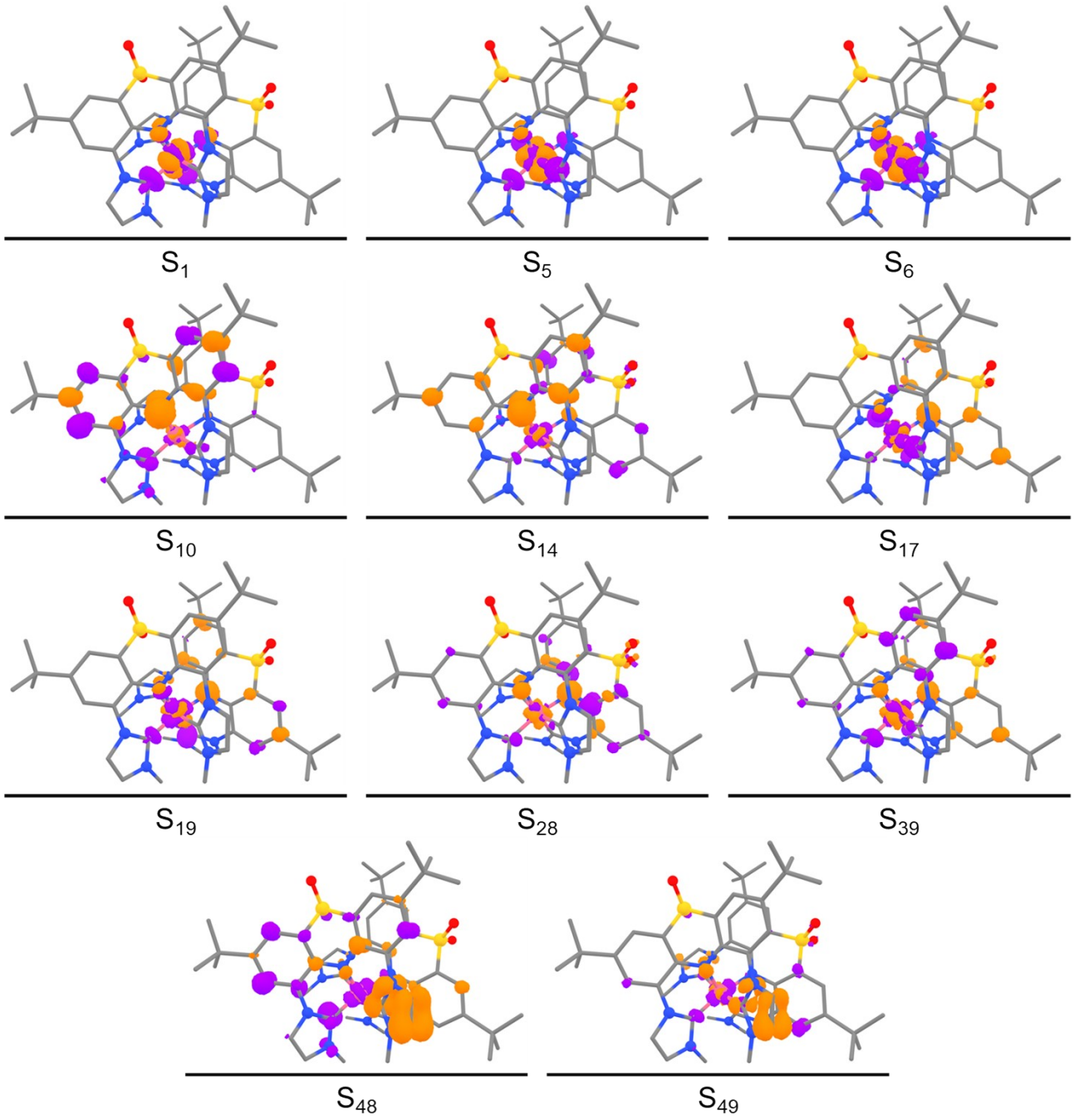

Figure S34. Electron density difference plot for S_n of **$CoSO_2$** from Table S8, respectively, based on TD-DFT calculations. Orange marks a depletion, and purple indicates a gain in electron density.

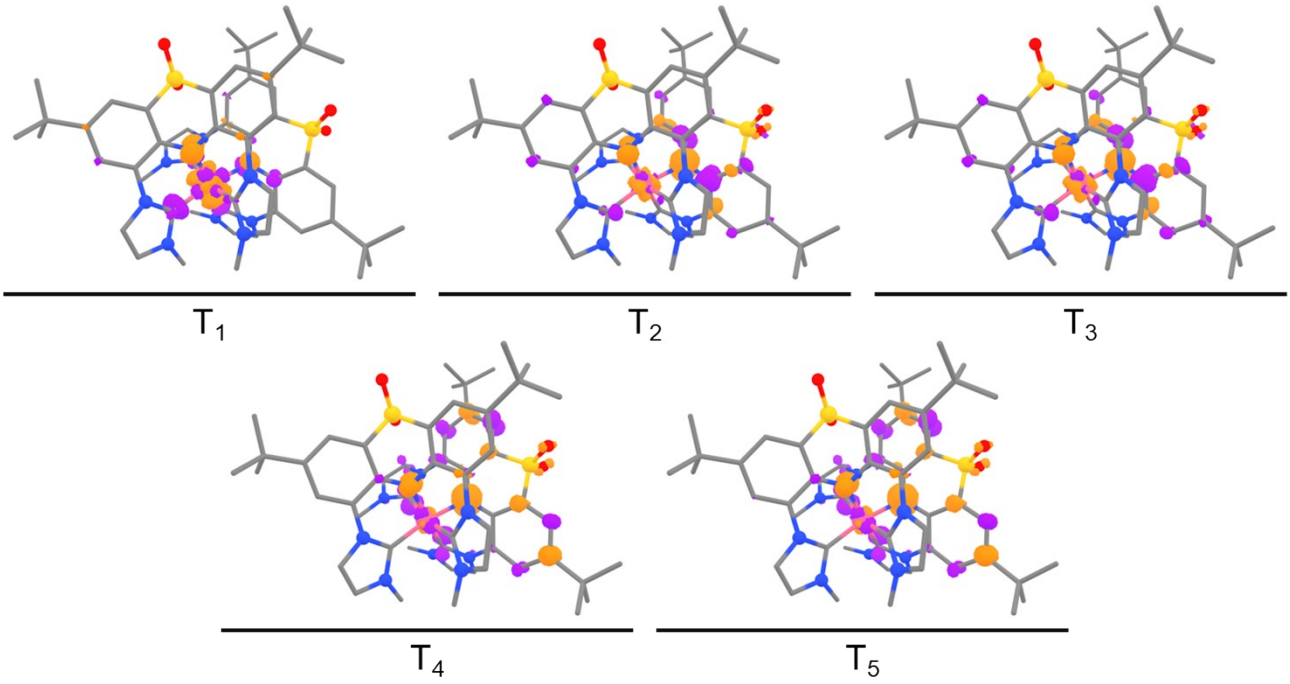

Figure S35. Electron density difference plot for T_n of **$CoSO_2$** from Table S9, respectively, based on SOC-TD-DFT calculations. Orange marks a depletion, and purple indicates a gain in electron density.

Cyclic voltammetry data

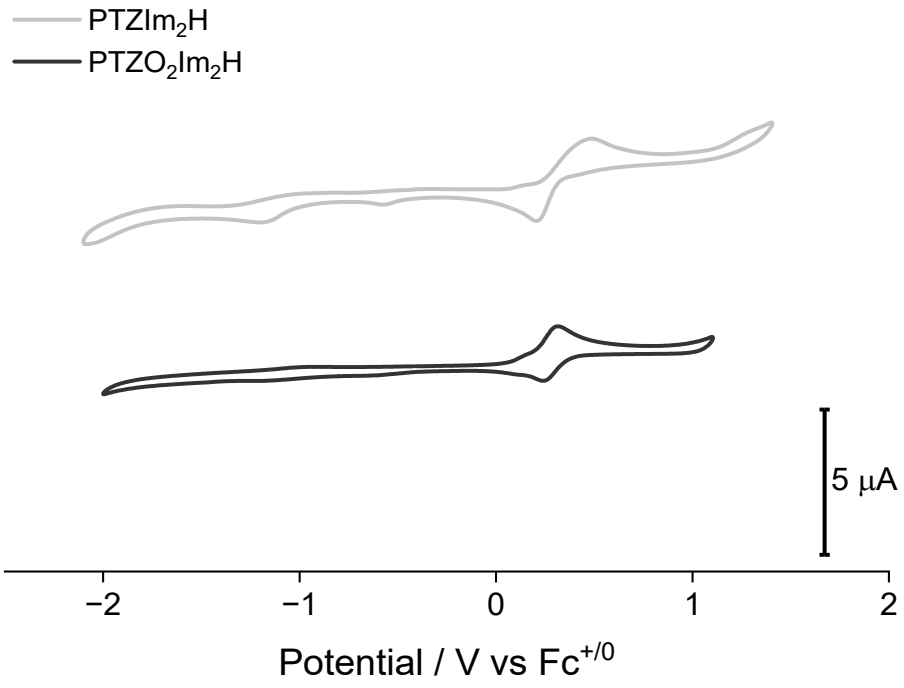

Figure S36. Cyclic voltammograms of **$PTZIm_2H$** and **$PTZO_2Im_2H$** in argon-sparged dry acetonitrile in 0.1 mol L^{-1} ($^nBu_4N$)PF_6, measured at a scan rate of 100 mV s^{-1}.

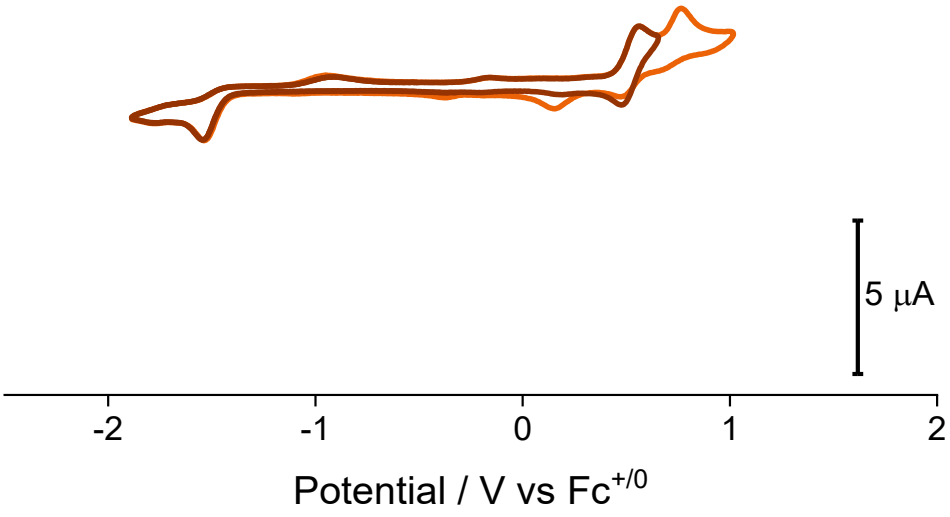

Figure S37. Cyclic voltammograms of **$CoSO_2$** in argon-sparged dry acetonitrile in 0.1 mol L^{-1} ($^nBu_4N$)PF_6, measured at a scan rate of 100 mV s^{-1} at different scanning windows.

Spectroelectrochemistry data

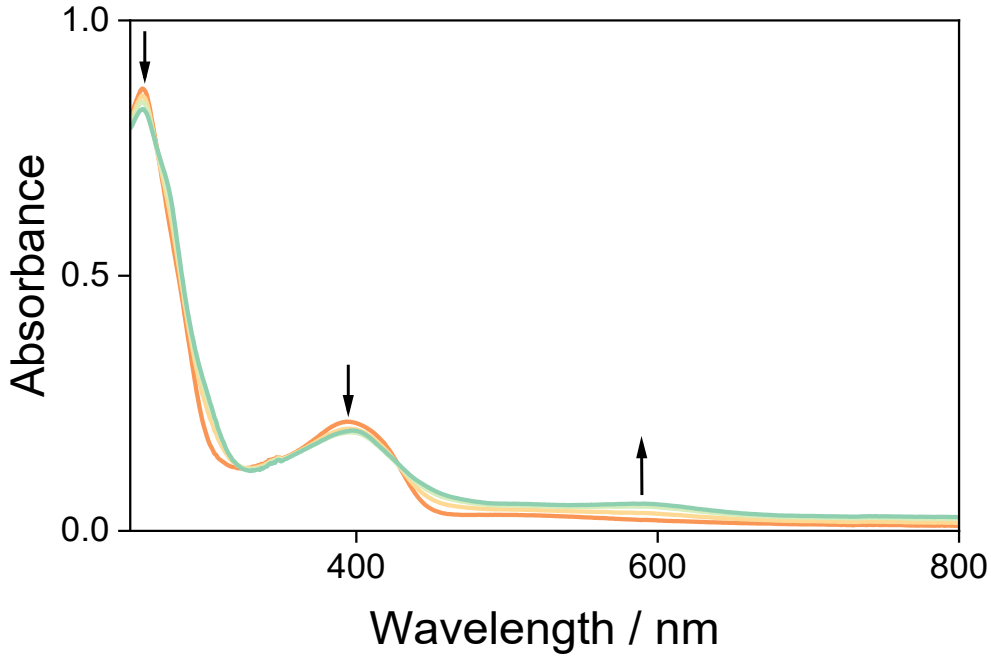

Figure S38. UV-vis changes upon electrochemical (ligand) oxidation of **CoS** scanning from −0.60 to −0.02 V vs $Fc^{+/0}$ in argon-sparged dry acetonitrile at a scan rate of 10 mV s^{-1}. The electrolyte was 0.1 M ($^{n}Bu_4N)PF_6$.

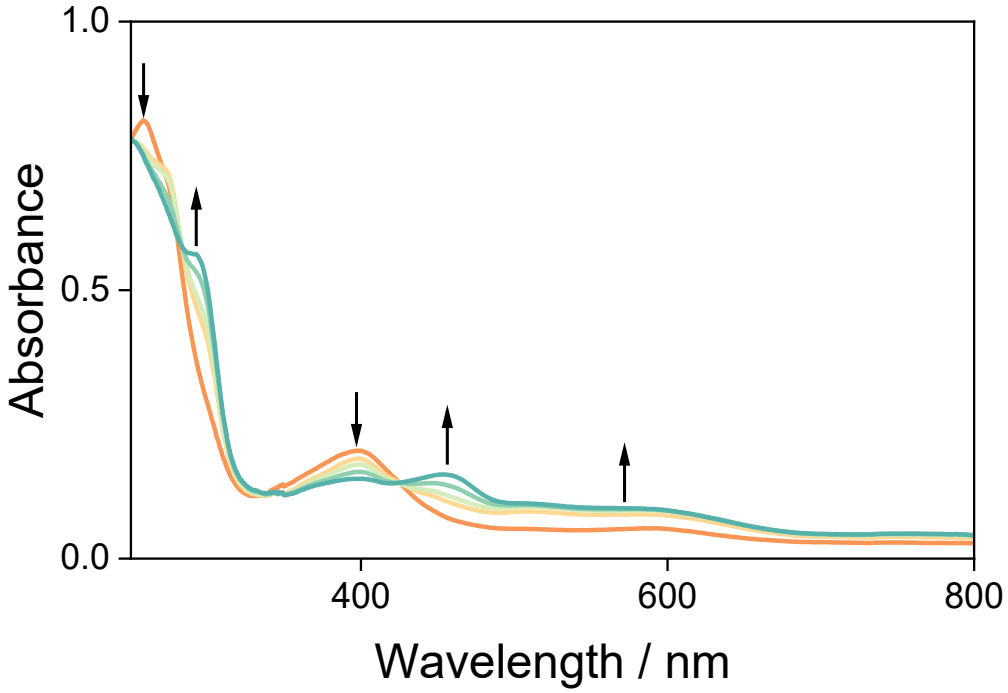

Figure S39. UV-vis changes upon electrochemical (metal) oxidation of **CoS** scanning from –0.02 to +0.40 V vs $Fc^{+/0}$ in argon-sparged dry acetonitrile at a scan rate of 10 mV s^{-1}. The electrolyte was 0.1 M ($^{n}Bu_4N)PF_6$.

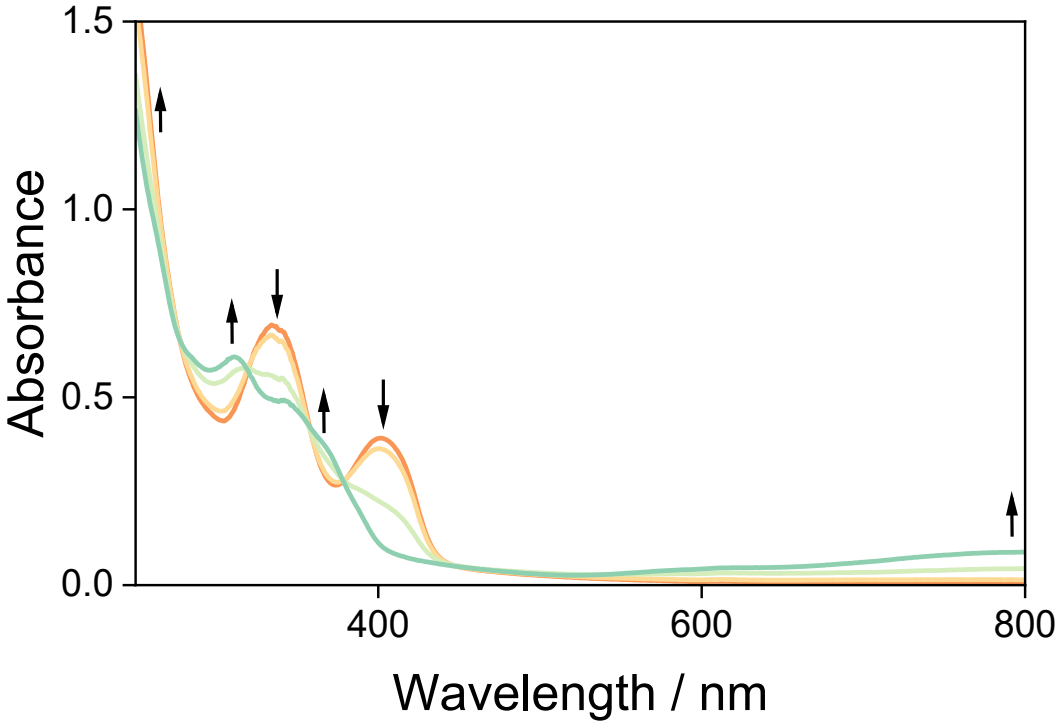

Figure S40. UV-vis changes upon electrochemical (ligand) oxidation of **$CoSO_2$** scanning from 0 to +0.70 V vs $Fc^{+/0}$ in argon-sparged dry acetonitrile at a scan rate of 10 mV s^{-1}. The electrolyte was 0.1 M ($^{n}Bu_4N$)PF_6.

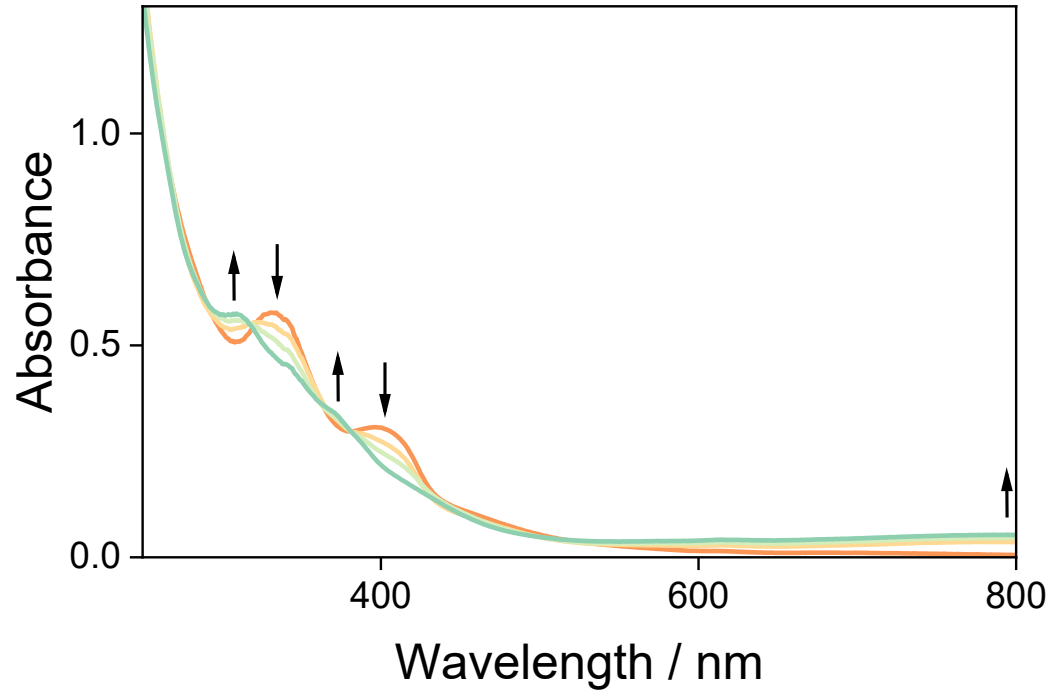

Figure S41. UV-vis changes upon electrochemical (ligand) reduction of **$CoSO_2$** scanning from 0 to −1.80 V vs $Fc^{+/0}$ in argon-sparged dry acetonitrile at a scan rate of 10 mV s^{-1}. The electrolyte was 0.1 M ($^{n}Bu_4N$)PF_6.

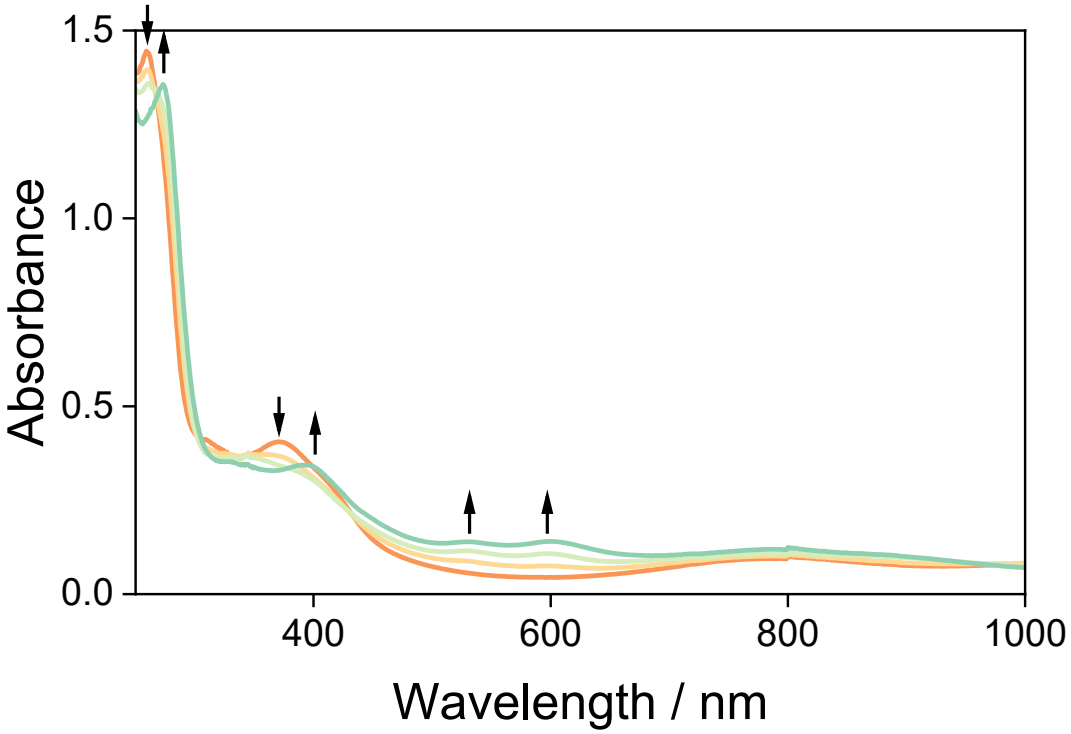

Figure S42. UV-vis changes upon electrochemical (ligand) oxidation of **FeS** scanning from −0.60 to +0.04 V vs $Fc^{+/0}$ in argon-sparged dry acetonitrile at a scan rate of 10 mV s^{-1}. The electrolyte was 0.1 M ($^{n}Bu_4N$)PF_6.

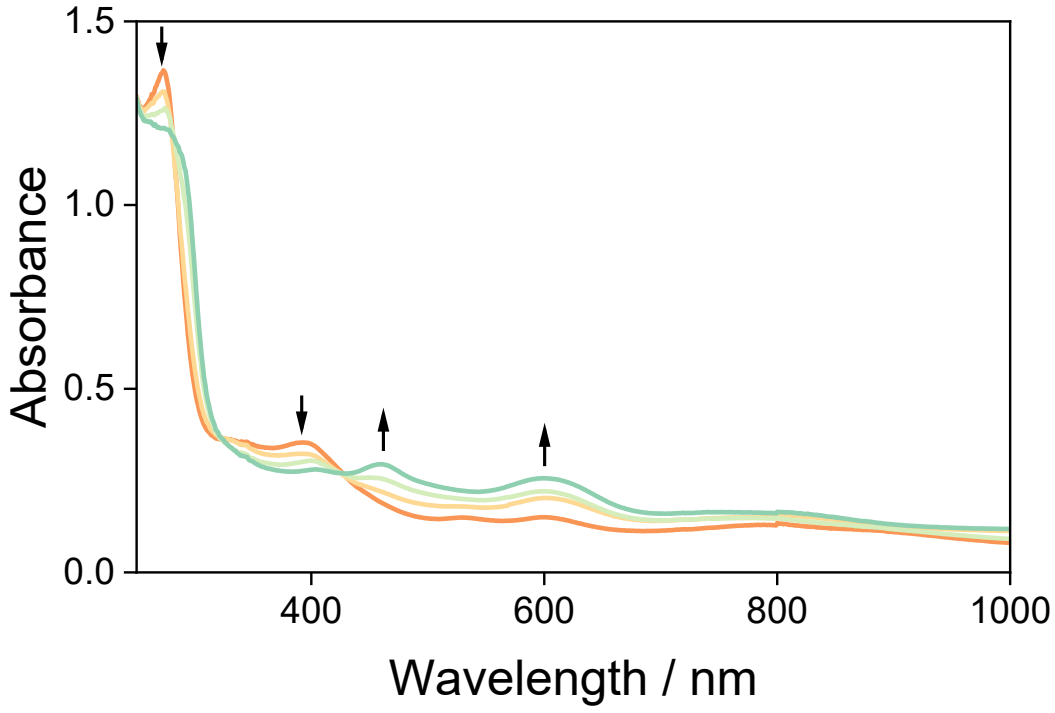

Figure S43. UV-vis changes upon electrochemical (metal) oxidation of **FeS** scanning from +0.04 to +0.40 V vs $Fc^{+/0}$ in argon-sparged dry acetonitrile at a scan rate of 10 mV s^{-1}. The electrolyte was 0.1 M ($^{n}Bu_4N$)PF_6.

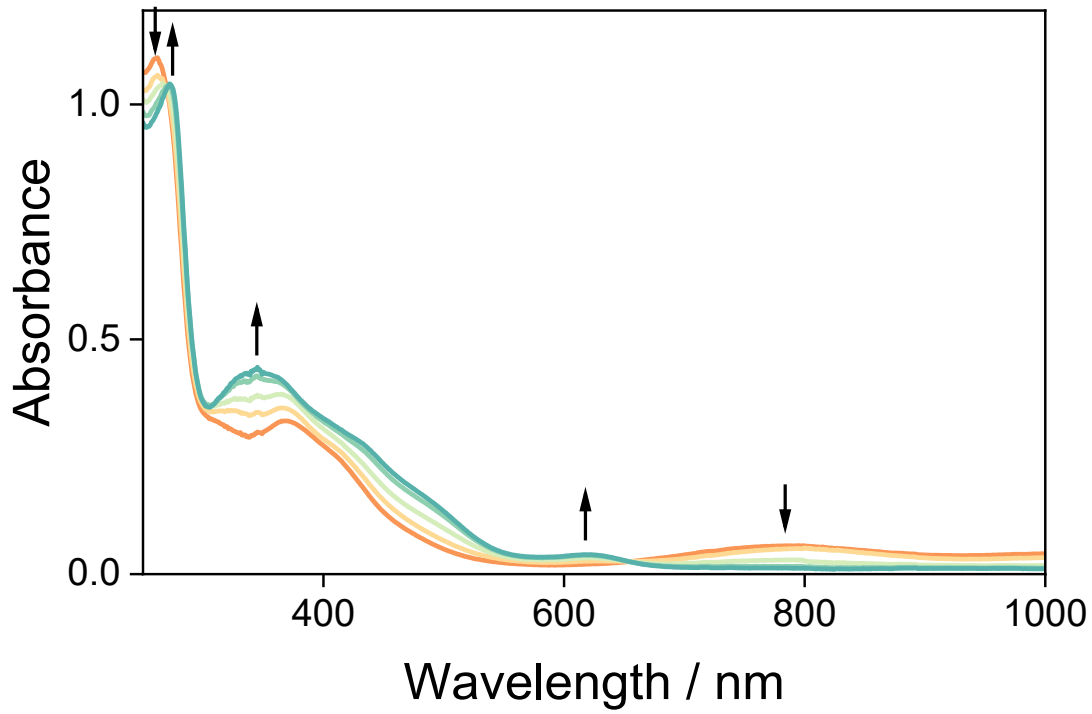

Figure S44. UV-vis changes upon electrochemical (metal) reduction of **FeS** scanning from −0.60 to −1.80 V vs $Fc^{+/0}$ in argon-sparged dry acetonitrile at a scan rate of 10 mV s^{-1}. The electrolyte was 0.1 M ($^{n}Bu_4N$)PF_6.

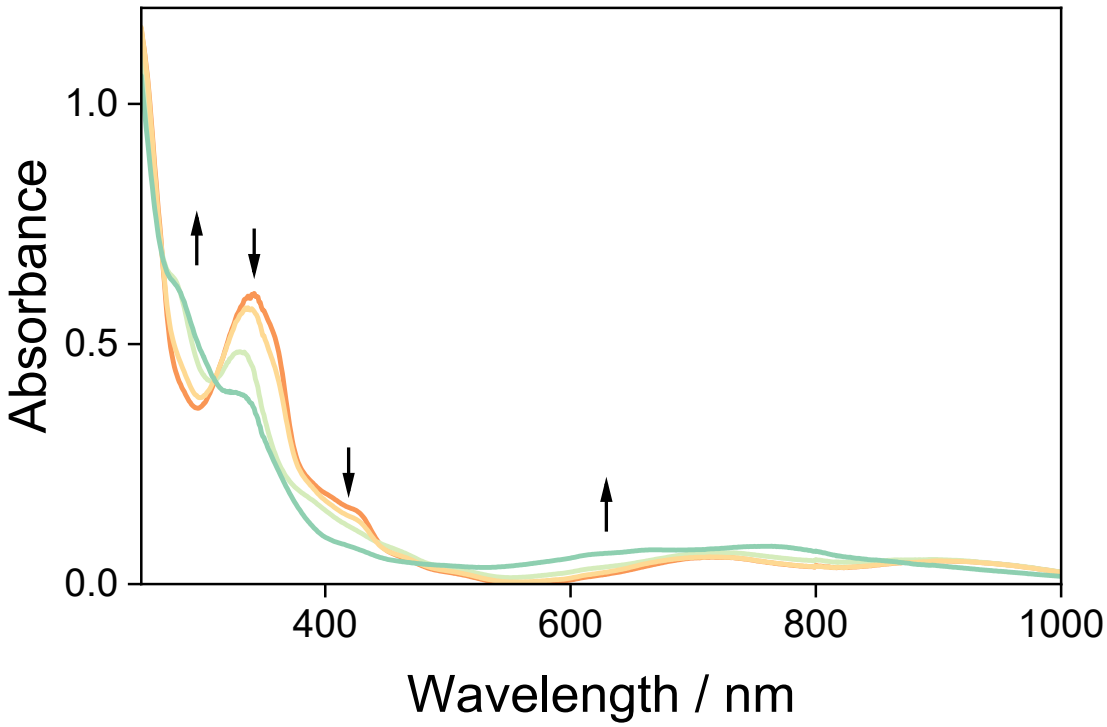

Figure S45. UV-vis changes upon electrochemical (ligand) oxidation of **$FeSO_2$** scanning from 0 to +0.70 V vs $Fc^{+/0}$ in argon-sparged dry acetonitrile at a scan rate of 10 mV s^{-1}. The electrolyte was 0.1 M ($^{n}Bu_4N$)PF_6.

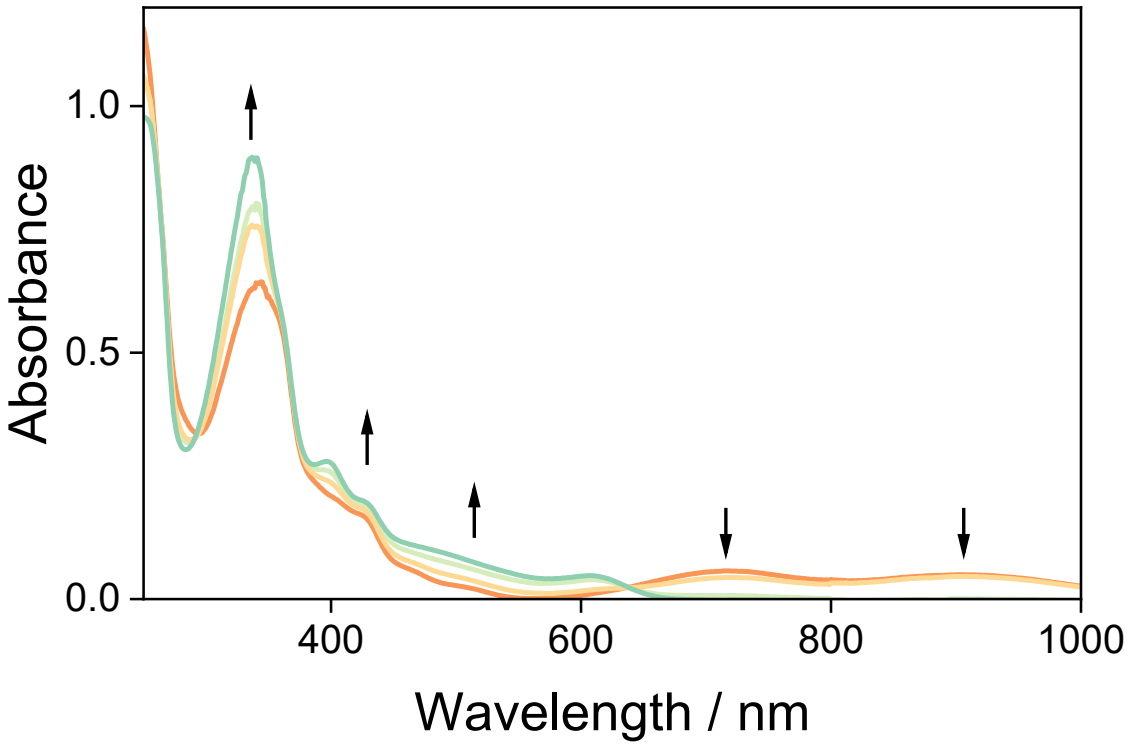

Figure S46. UV-vis changes upon electrochemical (metal) reduction of **$FeSO_2$** scanning from 0 to −1.00 V vs $Fc^{+/0}$ in argon-sparged dry acetonitrile at a scan rate of 10 mV s^{-1}. The electrolyte was 0.1 M ($^{n}Bu_4N$)PF_6.

Transient absorption spectroscopy data

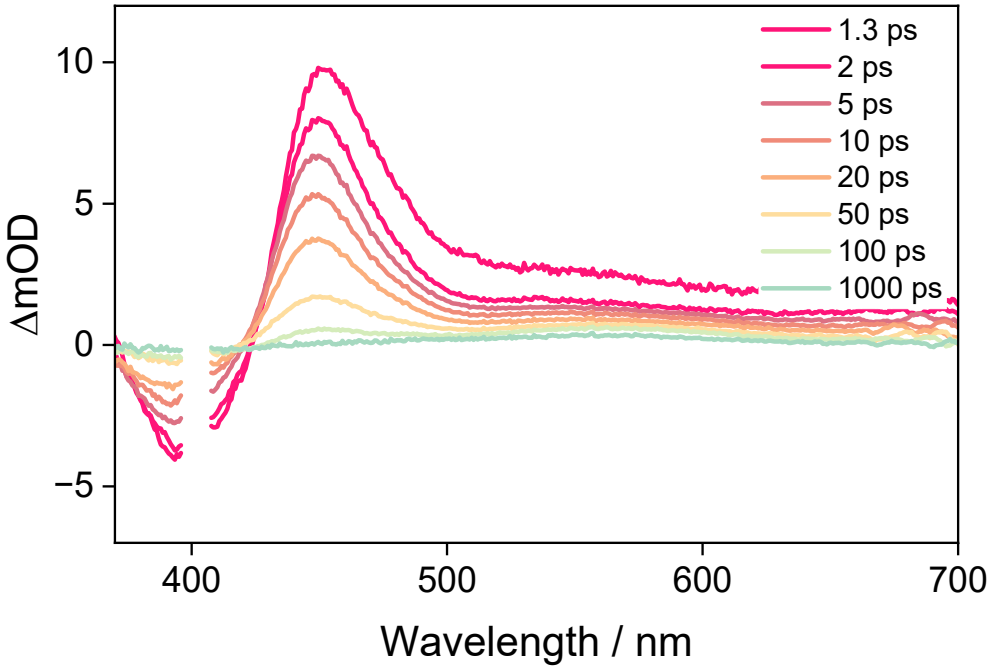

Figure S47. Femtosecond transient absorption spectra of **CoS** with various time delays in de-aerated acetonitrile at 298 K prompted by a 400 nm excitation source.

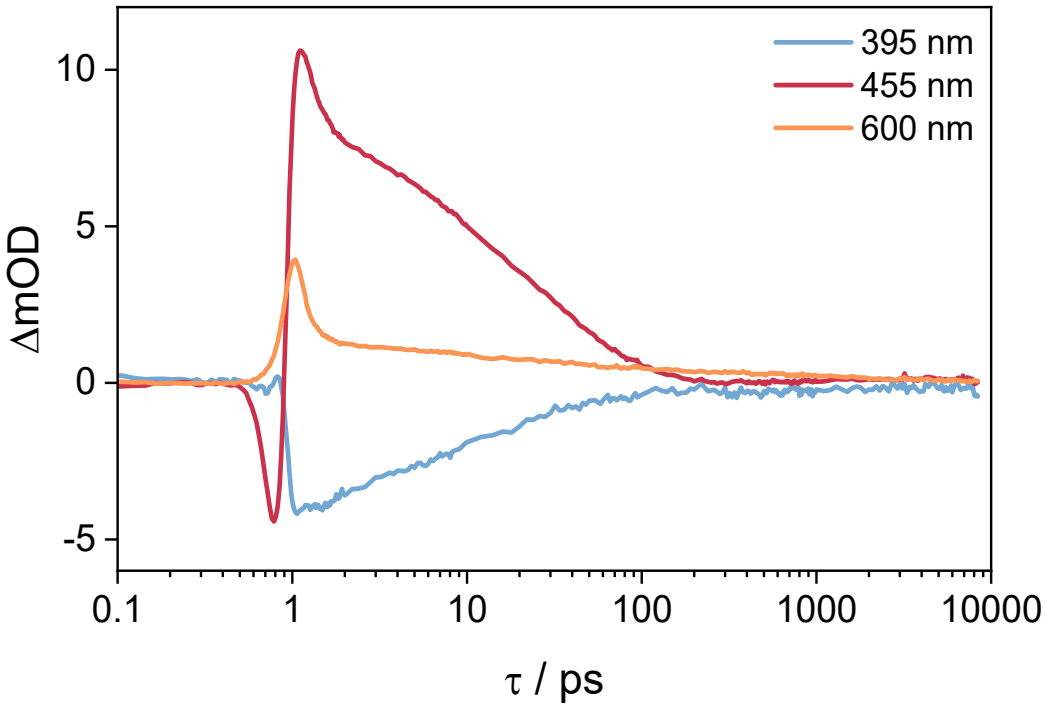

Figure S48. Kinetics of the ESA decay and GSB recovery at of **CoS** in de-aerated acetonitrile at 298 K obtained from femtosecond transient absorption.

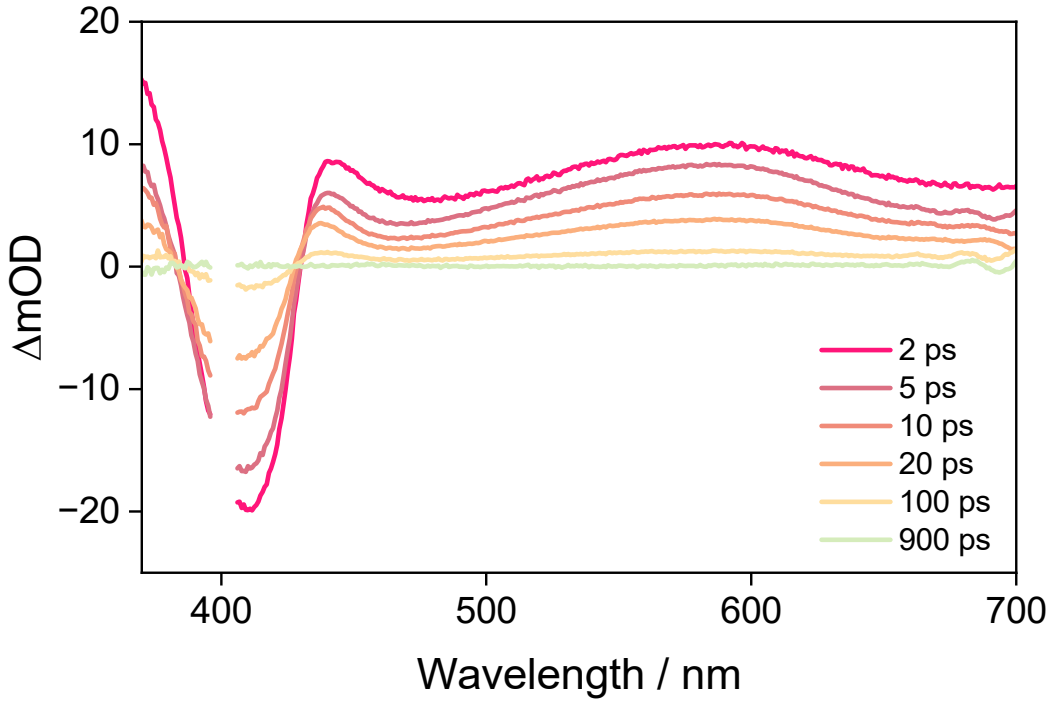

Figure S49. Femtosecond transient absorption spectra of **$CoSO_2$** with various time delays in de-aerated acetonitrile at 298 K prompted by a 400 nm excitation source.

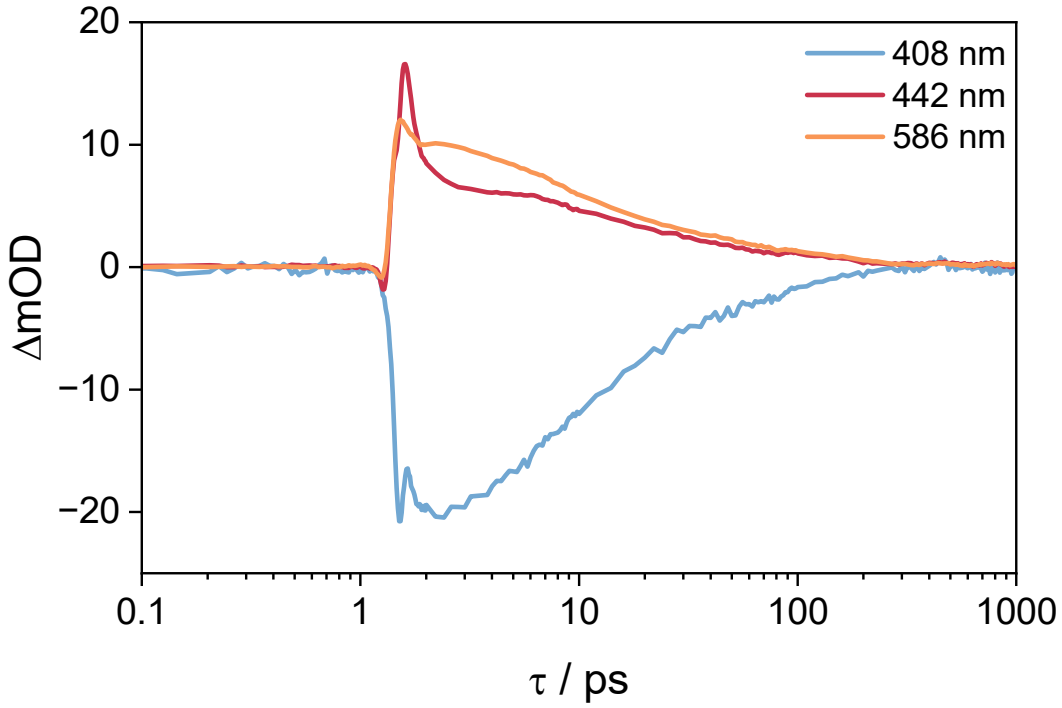

Figure S50. Kinetics of the ESA decay and GSB recovery at of **$CoSO_2$** in de-aerated acetonitrile at 298 K obtained from femtosecond transient absorption.

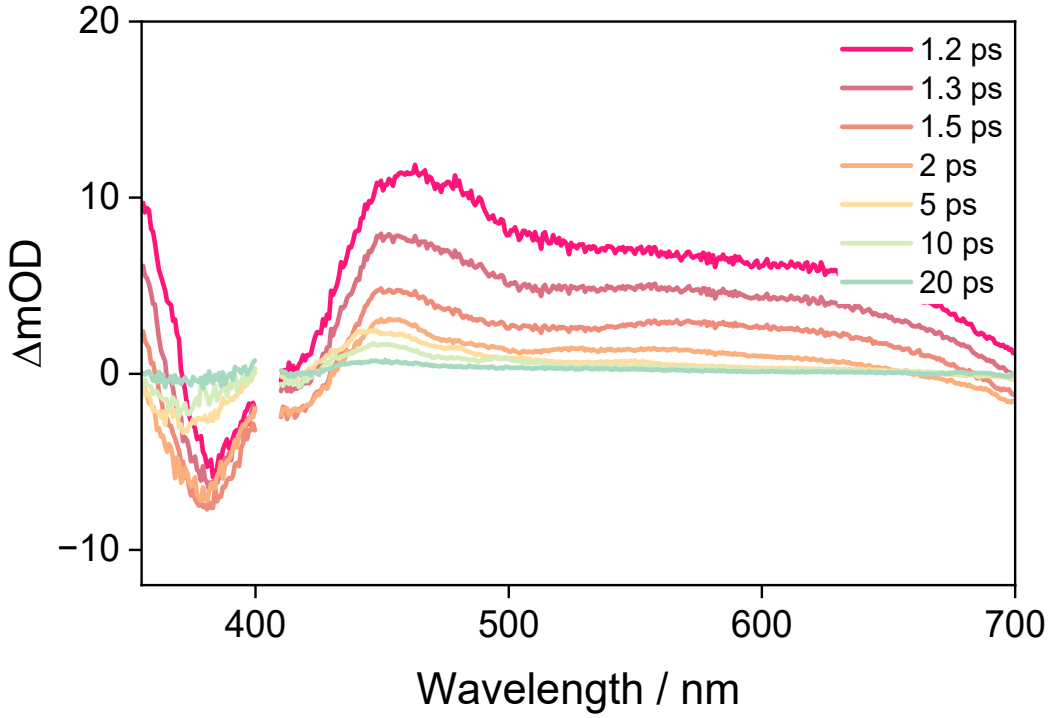

Figure S51. Femtosecond transient absorption spectra of **FeS** with various time delays in de-aerated acetonitrile at 298 K prompted by a 400 nm excitation source.

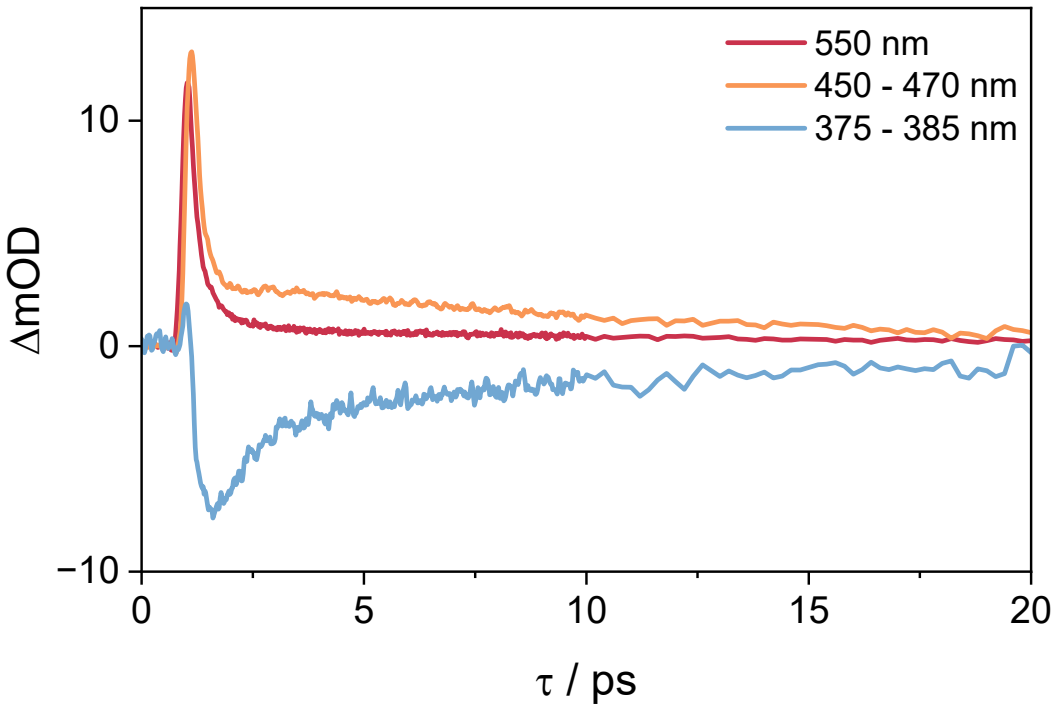

Figure S52. Kinetics of the ESA decay and GSB recovery at of **FeS** in de-aerated acetonitrile at 298 K obtained from femtosecond transient absorption.

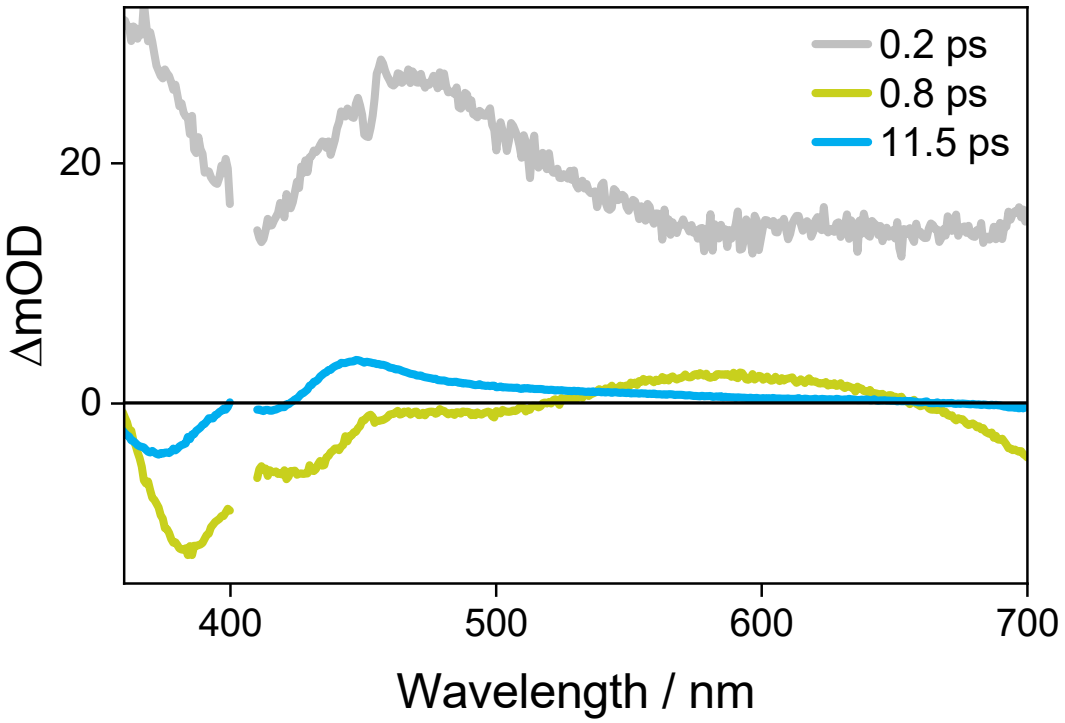

Figure S53. Decay-associated spectra (DAS) of **FeS** obtained from femtosecond transient absorption in de-aerated acetonitrile at 298 K prompted by a 400 nm excitation source.

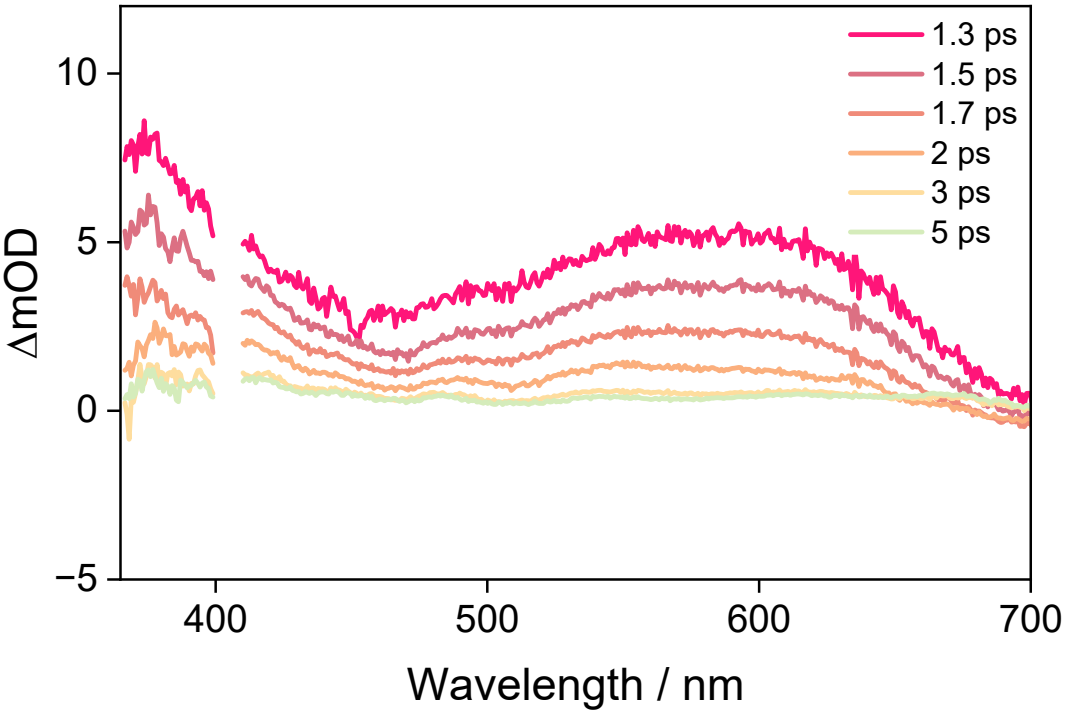

Figure S54. Femtosecond transient absorption spectra of **$FeSO_2$** with various time delays in de-aerated acetonitrile at 298 K prompted by a 400 nm excitation source.

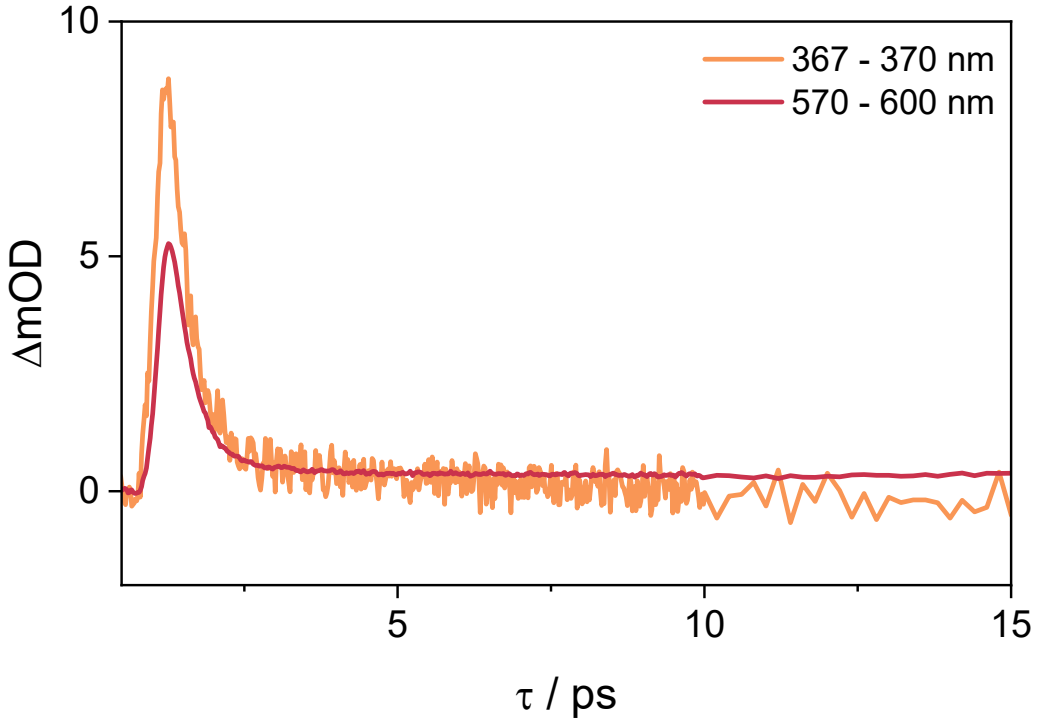

Figure S55. Kinetics of the ESA decay and GSB recovery at of **$FeSO_2$** in de-aerated acetonitrile at 298 K obtained from femtosecond transient absorption.

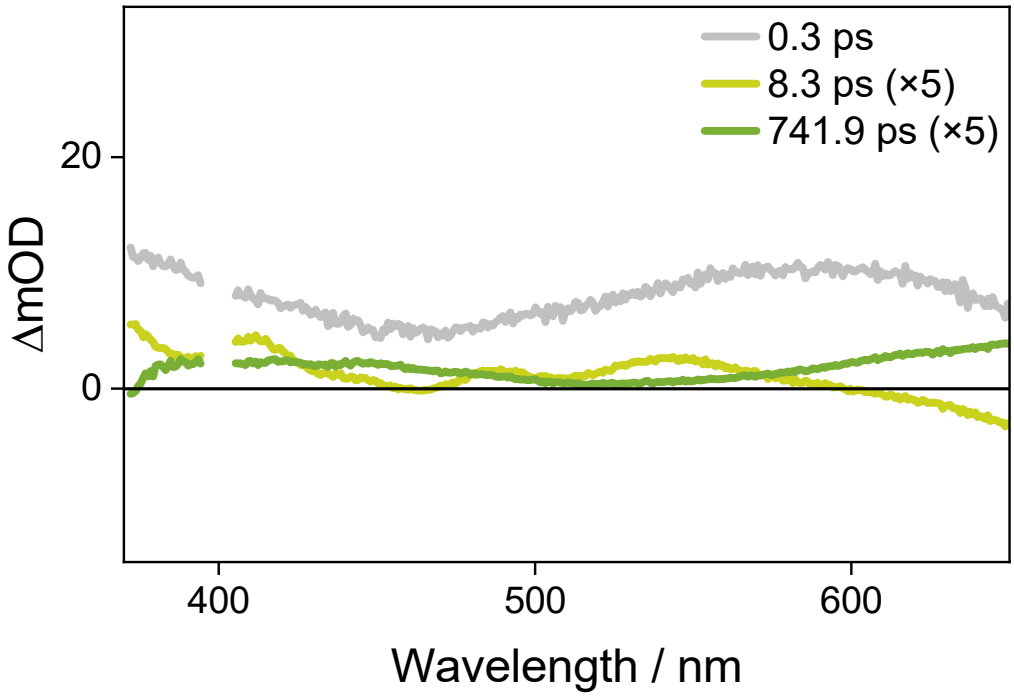

Figure S56. Decay-associated spectra (DAS) of **$FeSO_2$** obtained from femtosecond transient absorption in de-aerated acetonitrile at 298 K prompted by a 400 nm excitation source.

References

(1) Stoll, S.; Schweiger, A. EasySpin, a Comprehensive Software Package for Spectral Simulation and Analysis in EPR. *J. Magn. Reson.* **2006**, *178* (1), 42–55.
(2) Bruker, A. I. SAINT, Version 8.40B, 2019.
(3) Krause, L.; Herbst-Irmer, R.; Sheldrick, G. M.; Stalke, D. Comparison of Silver and Molybdenum Microfocus X-Ray Sources for Single-Crystal Structure Determination. *J. Appl. Crystallogr.* **2015**, *48* (Pt 1), 3–10.
(4) Dolomanov, O. V.; Bourhis, L. J.; Gildea, R. J.; Howard, J. a. K.; Puschmann, H. OLEX2: A Complete Structure Solution, Refinement and Analysis Program. *J. Appl. Crystallogr.* **2009**, *42* (2), 339–341.
(5) Sheldrick, G. M. Crystal Structure Refinement with SHELXL. *Acta Crystallogr. Sect. C Struct. Chem.* **2015**, *71* (Pt 1), 3–8.
(6) Krejčik, M.; Daněk, M.; Hartl, F. Simple Construction of an Infrared Optically Transparent Thin-Layer Electrochemical Cell: Applications to the Redox Reactions of Ferrocene, $Mn_2(CO)_{10}$ and $Mn(CO)_3$(3,5-Di-t-Butyl-Catecholate)$^-$. *J. Electroanal. Chem. Interfacial Electrochem.* **1991**, *317* (1), 179–187.
(7) Neese, F. Software Update: The ORCA Program System—Version 5.0. *WIREs Comput. Mol. Sci.* **2022**, *12* (5), e1606.
(8) Becke, A. D. Density-Functional Exchange-Energy Approximation with Correct Asymptotic Behavior. *Phys. Rev. A* **1988**, *38* (6), 3098–3100.
(9) Lee, C.; Yang, W.; Parr, R. G. Development of the Colle-Salvetti Correlation-Energy Formula into a Functional of the Electron Density. *Phys. Rev. B* **1988**, *37* (2), 785–789.
(10) Schäfer, A.; Huber, C.; Ahlrichs, R. Fully Optimized Contracted Gaussian Basis Sets of Triple Zeta Valence Quality for Atoms Li to Kr. *J. Chem. Phys.* **1994**, *100* (8), 5829–5835.
(11) Weigend, F.; Ahlrichs, R. Balanced Basis Sets of Split Valence, Triple Zeta Valence and Quadruple Zeta Valence Quality for H to Rn: Design and Assessment of Accuracy. *Phys. Chem. Chem. Phys.* **2005**, *7* (18), 3297–3305.
(12) Grimme, S.; Antony, J.; Ehrlich, S.; Krieg, H. A Consistent and Accurate Ab Initio Parametrization of Density Functional Dispersion Correction (DFT-D) for the 94 Elements H-Pu. *J. Chem. Phys.* **2010**, *132* (15), 154104.
(13) Grimme, S.; Ehrlich, S.; Goerigk, L. Effect of the Damping Function in Dispersion Corrected Density Functional Theory. *J. Comput. Chem.* **2011**, *32* (7), 1456–1465.
(14) Tomasi, J.; Mennucci, B.; Cammi, R. Quantum Mechanical Continuum Solvation Models. *Chem. Rev.* **2005**, *105* (8), 2999–3094.
(15) Petrenko, T.; Kossmann, S.; Neese, F. Efficient Time-Dependent Density Functional Theory Approximations for Hybrid Density Functionals: Analytical Gradients and Parallelization. *J. Chem. Phys.* **2011**, *134* (5), 054116.
(16) de Souza, B.; Neese, F.; Izsák, R. On the Theoretical Prediction of Fluorescence Rates from First Principles Using the Path Integral Approach. *J. Chem. Phys.* **2018**, *148* (3), 034104.
(17) ChemCraft 1.8.
(18) Sigmund, L. M.; Ebner, F.; Jöst, C.; Spengler, J.; Gönnheimer, N.; Hartmann, D.; Greb, L. An Air-Stable, Neutral Phenothiazinyl Radical with Substantial Radical Stabilization Energy. *Chem. Eur. J.* **2020**, *26* (14), 3152–3156.
(19) Sinha, N.; Pfund, B.; Wegeberg, C.; Prescimone, A.; Wenger, O. S. Cobalt(III) Carbene Complex with an Electronic Excited-State Structure Similar to Cyclometalated Iridium(III) Compounds. *J. Am. Chem. Soc.* **2022**, *144* (22), 9859–9873.